GeoScienceWorld
Lithosphere
Volume 2023, Article ID 7919174, 21 pages
https://doi.org/10.2113/2023/7919174

Lithosphere

Research Article

Holocene Earthquake Cycles of an Active Tectonic Block Boundary Fault Zone: A Case Study in the Qilian–Haiyuan Fault Zone, Northeastern Tibet Plateau

Shumin Liang,[1,2,3] Wenjun Zheng,[1,2] Dongli Zhang,[1,2] Hui Peng,[1,2] Xin Sun,[1,2] and Shiqi Wei[1,2]

[1]*Guangdong Provincial Key Laboratory of Geodynamics and Geohazards, School of Earth Sciences and Engineering, Sun Yat-sen University, Guangzhou, 510275, China*
[2]*Southern Marine Science and Engineering Guangdong Laboratory (Zhuhai), Zhuhai, 519082, China*
[3]*Key Laboratory of Marine Mineral Resources, Ministry of Natural Resources, Guangzhou Marine Geological Survey, China Geological Survey, Guangzhou, 511400, China*

Correspondence should be addressed to Wenjun Zheng; zhengwenjun@mail.sysu.edu.cn

Received 10 October 2022; Accepted 18 July 2023; Published 17 August 2023

Academic Editor: Songjian Ao

Fault zones along active tectonic block boundaries are a significant source of devastating continental earthquakes. Strong earthquakes produce disruptions of sediment and induce characteristic sediments near the fault, which serve as valuable sedimentary evidence for identifying and dating of paleoearthquakes. In this study, we aimed to reconstruct the earthquake history of the Qilian–Haiyuan fault zone in the northeastern Tibetan Plateau during the Holocene. We reanalyzed forty-four trenches and used the sedimentary sequences, event indicators, and age constraints to determine the earthquake history. Our analysis revealed the paleoearthquakes of 6 subsidiary faults of the Qilian–Haiyuan fault zone with accurate event ages and rupture extents. Based on the spatial and temporal distributions of strong earthquakes since 10 ka, we identified five earthquake clusters around the central-eastern Qilian–Haiyuan fault zone including seven rupture cascades where the earthquakes migrated gradually from east to west. The existing seismic gap reveals that the latest migration may not yet be complete and suggests a high probability of $M \geq 7$ earthquakes occurring on the Jinqianghe fault, Maomaoshan fault, and the central part of the Lenglongling faults. We concluded that, in order to better understand earthquake cycles and seismic hazards, it is important to consider a fault zone as a whole, including multiple faults and their interaction on the earthquake triggering between nearby faults.

1. Introduction

Large earthquakes concentrate at the boundaries of tectonic plates, which usually manifest in continents as large-scale fault systems comprising multiple interacting faults. Clustered behavior of strong earthquakes is a distinct and persistent feature of seismic activity over a long-time period in these fault systems [1–3]. Since this phenomenon was first discovered [4], it has become widely recognized that strong earthquakes can trigger earthquakes on adjacent faults. Changes in Coulomb stress offer a physical explanation for the clustering and migration of earthquakes [4–8]. The tectonic deformation of mainland China has been dominated by active-tectonic blocks since the late Quaternary [9–12]. Almost all of the $M > 7$ earthquakes within mainland China have occurred in block-boundary regions [13, 14]. Accommodating the relative motion between active blocks, the block-boundary fault zones are the main areas for the buildup and release of strain in strong earthquakes [15, 16]. Evidently, studying the pattern of earthquakes over time is crucial in predicting future earthquake events.

Investigating multiple earthquake cycles, paleoearthquake studies provide key insights into the seismic behavior of faults [17–21]. Trenching plays a crucial role in paleoearthquake studies, in which the age determination of prehistorical earthquakes is based on the identification and dating of coseismic sedimentary records [22–24]. A common method for determining the age of earthquakes compares the timings of paleoearthquakes in different trenches. The estimated ages of an event from multiple trenches show little difference, and the most likely age of this event can be determined by the time window that is common to all the estimates or by the interval limited by the closest upper and lower bounds from different trenches [25, 26]. As the material base of event dating, trench sediments are very likely affected by the drainage basins from which the Quaternary unconsolidated sediments mostly originate. The sedimentary environments should be similar in the trenches of the same drainage basin [27, 28]; however, a large-scale fault zone over hundreds of kilometers extends through different drainage basins. Based on the Gulang fault, research has verified that paleoearthquake age constraints can be improved by accounting for the influences of multicatchment sedimentary environments to effectively enhance the completeness and reliability of the paleoearthquake sequence [29].

The Qilian–Haiyuan fault zone is the first-order block-boundary fault zone among the Alxa, Qaidam, and Ordos blocks in the northeastern Tibet Plateau (Figure 1) [15, 16, 30]. It comprises seven subsidiary faults. Located along the southern margin of Qilian Shan (mountain), the Qilian–Haiyuan fault zone spans a uniform climate and encompasses various drainage basins. Several destructive historical earthquakes have occurred in the Qilian–Haiyuan fault zone, including the *M* 6¾ Jingtai earthquake of 1888, the *M* 8½ Haiyuan earthquake of 1920, and the *M* 8 Gulang earthquake of 1927 (Figure 1) [31–36]. It has been proposed that the Gulang earthquake was affected by the Coulomb stress change resulting from the Haiyuan earthquake, and it was brought forward by 16–44 years [37]. The study of historical earthquakes covers only the most recent earthquake cycles. Coupled with an improved paleoseismic history constrained by sedimentary sequences of different drainage basins, this can provide a better understanding of the long-term seismic behavior and interaction of these faults over multiple earthquake cycles.

Extensive paleoearthquake research has been conducted in the Qilian–Haiyuan fault zone. These studies form the basis for our new multitrench event chronology concentrated on the trench sediments of different drainage basins. In this study, we assembled the results from forty-four trenches excavated in previous studies and built up their sedimentary sequences. These trenches are divided into different groups depending on fault segmentation and drainage basin delineation to establish multitrench composite sedimentary sequences through stratigraphic correlation. We identified the high-quality event indicators and used them to distinguish the very likely earthquakes from previously identified paleoearthquakes. The earthquake horizons for the very likely events and multitrench possible events in each catchment were identified with refined age estimates. Consequently, this allowed us to analyze the earthquake reoccurrence of both subsidiary faults and the Qilian–Haiyuan fault zone as a whole by integrating the event ages and rupture extents.

2. Geologic Setting

Responding to the northeastward growth of the Tibetan Plateau and impeded by the rigid Gobi Alashan block, the Qilian–Haiyuan fault zone acted as a northward-directed thrust fault in its early phase and then transitioned to a left-lateral strike slip during the middle to late Miocene [38–42]. Currently, the Qilian–Haiyuan fault zone is dominated by a left-lateral strike slip with a thrust component, striking NWW–SEE. The Qilian–Haiyuan fault zone starts near the Hala Hu (lake) in Qilian Shan in the west and ends in the Liupan Shan (mountain) in the east. It is composed of 7 subsidiary faults, including the Halahu, Tuolaishan, Lenglongling, Jinqianghe, Maomaoshan, Laohushan, and Haiyuan faults from west to east (Figure 1) [41, 43]. A slip rate of 1–2 mm/a has been suggested for the Halahu fault [44]. Slip rates are stable at 3–5 mm/a along the 600 km central part of this fault zone but decrease to 1–3 mm/a and even lower at the eastern end [43, 45, 46].

Several strong ground-rupturing earthquakes have occurred in the Qilian–Haiyuan fault zone (Figure 1). The *M* 6¾ Jingtai earthquake rupture in 1888 traversed the Laohushan and Xijishui basin segments of the Laohushan fault [47]. In 1920, the entire Haiyuan fault ruptured during the *M* 8.5 Haiyuan earthquake [31–33, 35]. The ~230-km-long surface rupture zone extended from Jingtai to Guyuan, resulting in a devastating earthquake that killed over 270,000 people [48]. Recently, an Ms 6.9 earthquake occurred in Menyuan, Qinghai in 2022. The main surface rupture of this earthquake had a total length of ~27 km, including the eastern end of the Tuolaishan fault and the western end of the Lenglongling fault [49, 50].

Many paleoearthquake trenches have been opened across the subsidiary faults in the Qilian–Haiyuan fault zone (Figures 1 and 2). On the Lenglongling fault, six recent paleoearthquakes were discovered in the trench excavations [51]. Yuan et al. [52] reported five *M* 7.5 events that are quasi-periodic on the Maomaoshan and Jinqianghe faults. Six paleoearthquakes were found on the Laohushan fault based on two trenches at the Songshan site [53]. Three, seven, and six events since 12 ka were reported in 3 segments, respectively, by a comprehensive trench investigation of the Haiyuan fault [54]. Unfortunately, the earthquake history of the Halahu and Tuolaishan faults remains unclear due to difficulty in accessing them.

The ~1000 km Qilian–Haiyuan fault zone spans several river systems with a large number of tributaries, such as the Hei He (river), Datong He, Zhuanglang He, Gulang He, Sitandasha He, Yellow River, and Qingshui He from west to east (Figures 1 and 2). The western–central Qilian–Haiyuan fault zone is mainly located on the southern margin of Qilian Shan amid large undulations of topography. Sand

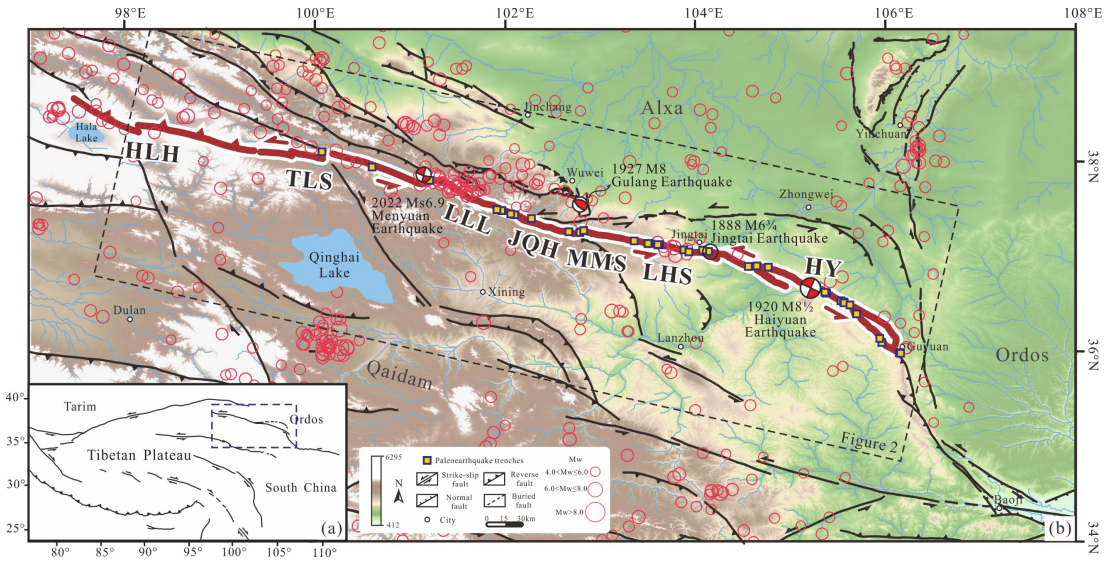

FIGURE 1: Seismotectonic setting and distribution map of the Qilian–Haiyuan fault zone. (a) The study area is on the northeastern margin of the Tibetan Plateau with the blue-dashed box indicating the position of panel b. (b) Main active faults on the northeastern margin of the Tibetan Plateau. The fault locations are modified from References 38, 51, 124, 125. The red lines represent the Qilian–Haiyuan fault zone. The seismic data (red circles) of $M \geq 4$ are from the United States Geological Survey (USGS) covering the period of 1960–2021, and the strong historical earthquakes (beach balls and black circle) are from References 34, 36, 49. The dashed box outlines Figure 2. Fault abbreviations: HLH = Halahu fault; TLS = Tuolaishan fault; LLL = Lenglongling fault; JQH = Jinqianghe fault; MMS = Maomaoshan fault; LHS = Laohushan fault; HY = Haiyuan fault.

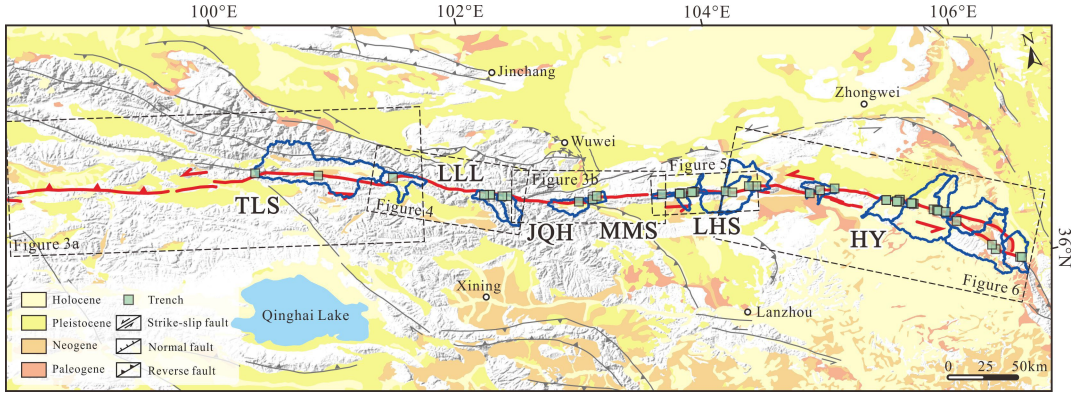

FIGURE 2: Cenozoic geological map surrounding the Qilian–Haiyuan fault zone. The blue lines indicate the drainage basins involving paleoearthquake trenches (green blocks). The dashed boxes from west to east display the locations of Figures 3(a), 4(a), 3(b), 5(a), and 6(a), respectively.

and gravel are derived from snowmelt and fluvial erosion at high altitudes and become the main components of the sediments near the faults along the mountain front. The eastern Qilian–Haiyuan fault zone enters the loess-covered northeastern Tibetan Plateau where the undulation of the topography is smaller. The sediments near the faults consist largely of loess, clay, silt, and sand, which are transported by large-scale alluvial systems.

Significant progress has been made in the study of paleoearthquakes along the Qilian–Haiyuan fault zone. However, these studies often only focus on individual subsidiary faults, resulting in a limited understanding of the long-term seismic behavior of the entire fault zone. This study primarily focuses on synthesizing large amounts of trench data systematically and reconstraining the strong earthquakes more accurately based on the sediments of different drainage basins.

3. Data and Methods

3.1. Data Source. Numerous paleoearthquake trench studies have been conducted on subsidiary faults of the Qilian–Haiyuan fault zone. We collected the results from forty-four trenches opened in the previous studies, which are shown in Figure 2 and Table 1 [47, 51–53, 55–75]. Unfortunately, no trench has been opened on the Halahu fault, and publicly available trench studies of the Tuolaishan, Jinqianghe, and Maomaoshan faults are limited. More trenches can be found on the fault sections that ruptured historically or are easily accessible

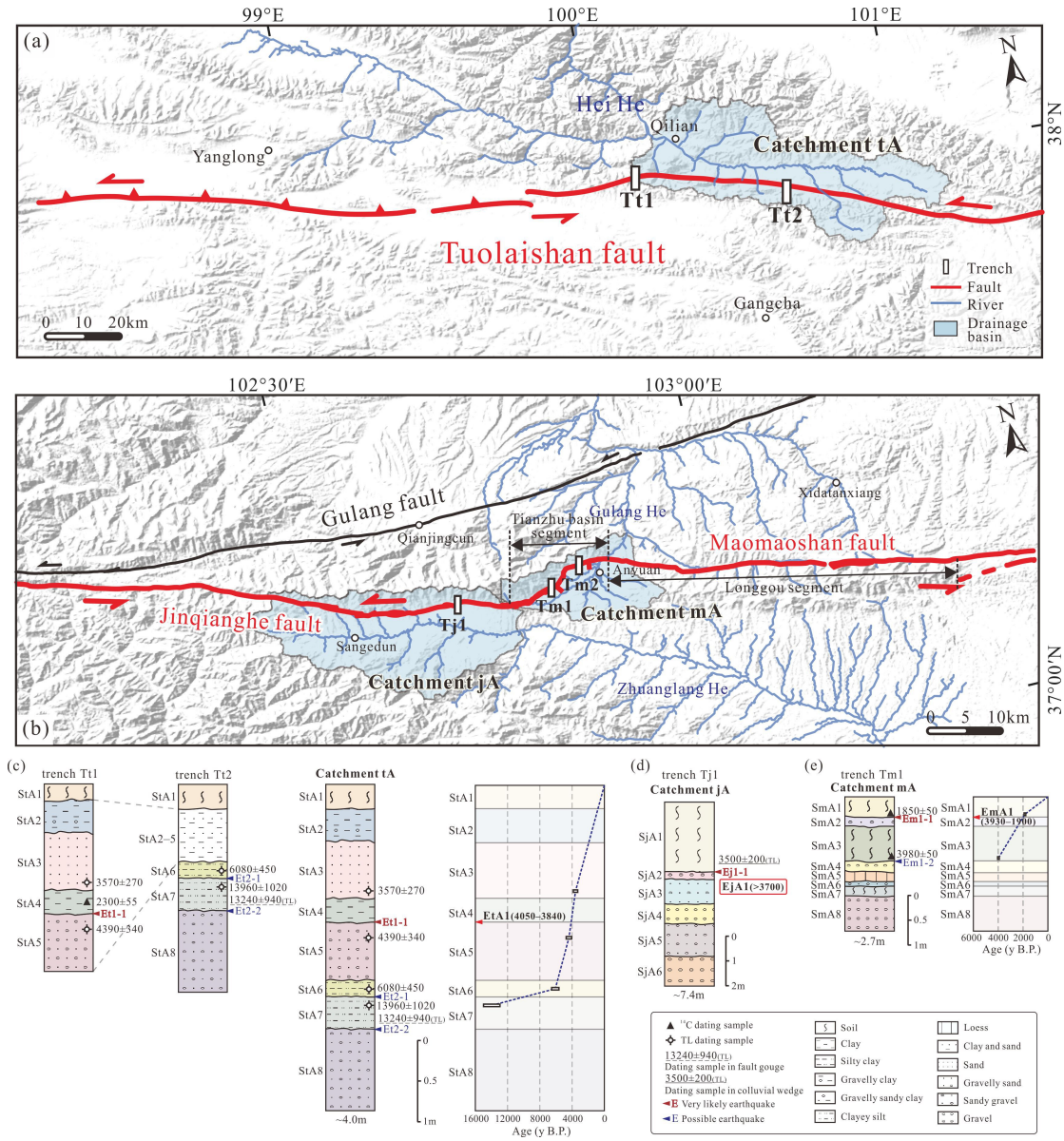

FIGURE 3: Paleoearthquake constraints for the Tuolaishan, Jinqianghe, and Maomaoshan faults. The map of the (a) Tuolaishan fault and (b) Jinqianghe and Maomaoshan faults shows the paleoearthquake trenches, fault structural segmentation, and drainage basins. The fault locations are from References 29, 124, 126. Single-trench sedimentary sequences and composite sedimentary sequences of multiple trenches in (c) Catchment tA, (d) Catchment jA, and (e) Catchment mA with the age framework and inferred ages of paleoearthquakes. The colored unit in the columns represents the one-to-one corresponding single-sedimentary unit during the stratigraphic correlation, while the white unit without further stratification in the references consists of more than 1 sedimentary unit.

by road, such as the eastern end of the Lenglongling fault and the Caoxia and Laohushan segments of the Laohushan fault. Six and ten trenches were used to capture the paleoearthquakes of the Lenglongling and Laohushan faults, respectively. The Haiyuan fault is subject to most research attention, owing to the infamous Haiyuan earthquake in 1920. Twenty-three trenches were opened, with a relatively uniform distribution spanning the entire fault. All trench logs and descriptions of these forty-four trenches from open-source studies were collected and analyzed to support our research.

3.2. Sedimentary Sequence Construction. Exposed sediment in trenches offers a material foundation and key geological evidence for paleoearthquake identification and is a sample source for event dating [18, 22–24]. Sediment is key in capturing capture the earthquake horizon and determines determining the timing of occurrence. To extract this key resource in each trench, a single-trench columnar sedimentary sequence was used to provide a real but simplified reflection of the trench sediment with previous dating results.

Almost all subsidiary faults of the Qilian-Haiyuan fault zone are dominated by left-lateral strike-slip. In the walls

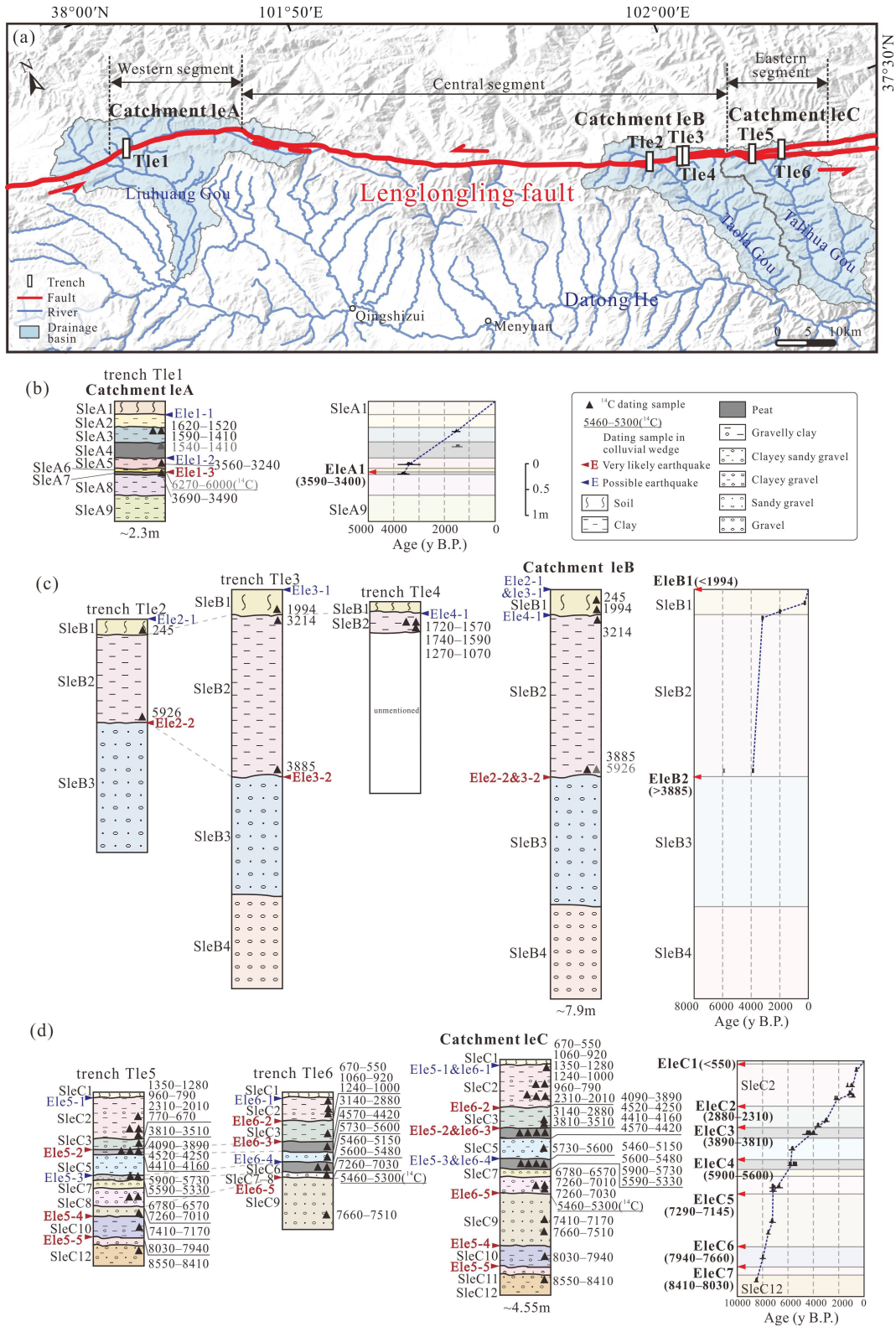

FIGURE 4: Paleoearthquake constraining on the Lenglongling fault. (a) Distribution map of the Lenglongling fault showing the paleoearthquake trenches, fault structural segmentation, and three drainage basins (Catchments leA to leC). The fault locations are from Reference 51. Single-trench sedimentary sequences and composite sedimentary sequences of multiple trenches in (b) Catchment leA, (c) Catchment leB, and (d) Catchment leC are shown with the age framework and inferred ages of paleoearthquakes. The colored unit in the columns represents the one-to-one corresponding single-sedimentary unit during the stratigraphic correlation, while the white unit has no sedimentary description or consists of more than one sedimentary unit. The ^{14}C ages in trenches Tle2 and Tle3 reported by Reference 57 are exact numbers rather than age ranges, the same as those shown here.

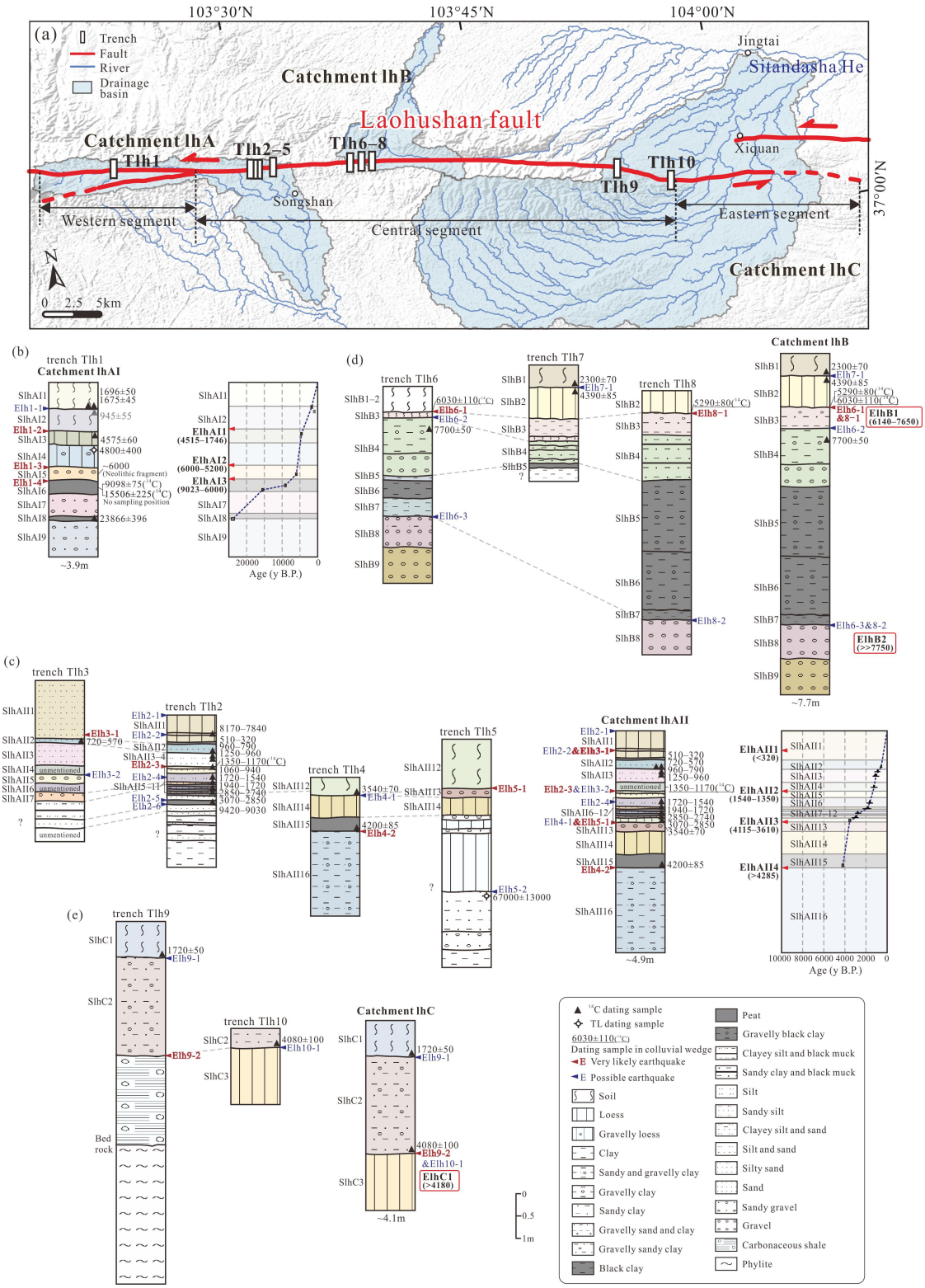

FIGURE 5: Paleoearthquake constraining the Laohushan fault. (a) Distribution map of the Laohushan fault showing paleoearthquake trenches, fault structural segmentation, and three drainage basins (Catchments lhA to lhC). The fault locations are from Reference 126. Single-trench sedimentary sequences and composite sedimentary sequences of multiple trenches in (b) Catchment lhAI, (c) Catchment lhAII, (d) Catchment lhBI, (e) Catchment lhBII, and (f) Catchment lhC with the age framework and inferred ages of paleoearthquakes. The colored unit in the columns represents the one-to-one corresponding single sedimentary unit during the stratigraphic correlation, while the white units are the bedrock, a composite unit consisting of more than 1 sedimentary unit, or the old units that are poorly matched with the units in other trenches.

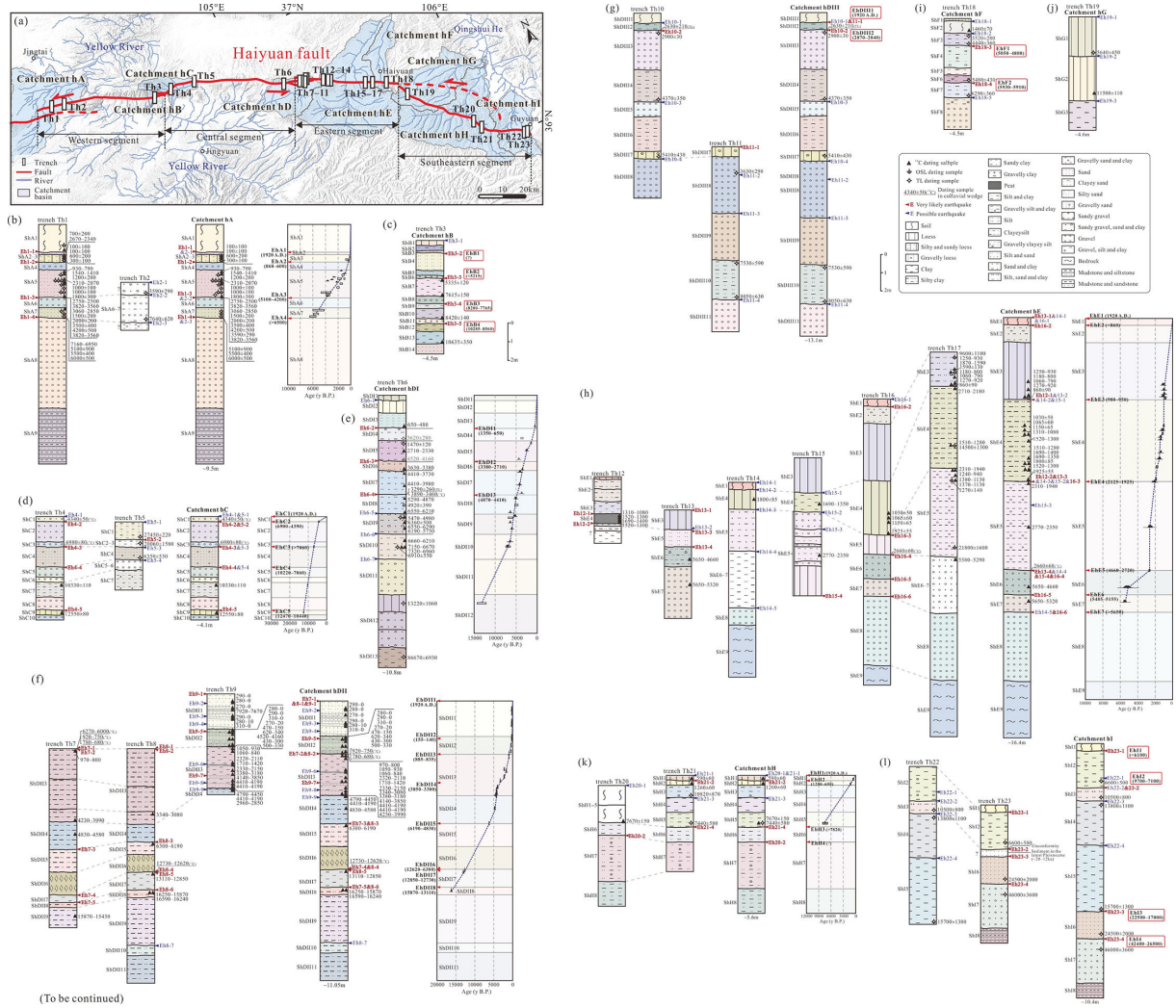

FIGURE 6: Paleoearthquake constraining the Haiyuan fault. (a) Distribution map of the Haiyuan fault showing the paleoearthquake trenches, fault structural segmentation, and three drainage basins (Catchments hA to hI). The fault locations are from Reference 127. Single-trench sedimentary sequences, composite sedimentary sequences of multiple trenches in (b) Catchment hA, (c) Catchment hB, (d) Catchment hC, (e) Catchment hDI, (f) Catchment hDII, (g) Catchment hDIII, (h) Catchment hE, (i) Catchment hF, (j) Catchment hG, (k) Catchment hH, and (l) Catchment hI with the age framework and inferred ages of paleoearthquakes. The colored unit in the columns represents the one-to-one corresponding single sedimentary unit during the stratigraphic correlation, while the white units are a composite unit consisting of more than 1 sedimentary unit or the units that are poorly matched with the units in other trenches.

of trenches, the fault is always recognized as an apparent reverse fault, normal fault, or fault zone containing multiple reverse or normal faults of different inclinations. The thickness and completeness of sediment on the downthrown side are assumed to be greater than that on the upthrown side. The sedimentary center is defined in a stable area a few meters from the fault, where the majority of sedimentary units have the greatest thickness. The sedimentary sequence was established by referring to the sedimentary center on the downthrown side of each trench. In some trenches where multiple sedimentary units are not laterally continuous, we tend to record the units with the greatest continuity and the largest number of dating samples to establish the sedimentary sequence. In addition, colluvial wedges, material filling opened fissures, and sediment ponded against a scarp are characteristic deposits caused by strong earthquakes. They are not a part of the stable sediment accumulation and, hence, would not be accounted for in the construction of a sedimentary sequence.

Sediment descriptions from paleoearthquake trenches in previous studies are usually very detailed. They may include color, lithology, grain size, psephicity, grading, bedding, marker sediment or layers (lens, peat block, gravel band, etc.), local deformation, and internal detailed stratification. We simplified these descriptions to be sufficiently representative yet easily displayed in columnar sedimentary sequences and differentiated during stratigraphic correlation.

The dating samples were placed in the sampled sedimentary unit according to the sampling depth mentioned in the references or the distance between the unit top plane and the sample shown in the sketch of

Table 1: Forty-four trenches of the Qilian–Haiyuan fault zone.

Fault	Trench no.	Trench name	Fault segment	Drainage basin	Geomorphic unit	Reference
Tuolaishan	Tt1	Dongcaohe	—	Catchment tA	River terrace	[55]
	Tt2	Xiaobabaohe	—	Catchment tA	Mountain ridge	[55]
Lenglongling	Tle1	Liuhuanggou	Western	Catchment leA	River terrace	[56]
	Tle2	Western taolachailong	Central	Catchment leB	Mountain ridge	[57]
	Tle3	Taolachailong 1	Central	Catchment leB	River terrace	[57]
	Tle4	Taolachailong 2	Central	Catchment leB	River bank	[58]
	Tle5	Talihuagou	Eastern	Catchment leC	River terrace	[51]
	Tle6	Niutougou	Eastern	Catchment leC	River terrace	[51]
Jinqianghe	Tj1	Hazhanggou	—	Catchment jA	River terrace	[52]
Maomaoshan	Tm1	Shangjiaodonggou	Tianzhu Basin	Catchment mA	River terrace	[59]
	Tm2	Eastern Lijiazhuang	Tianzhu Basin	Catchment mA	River bank	[59]
Laohushan	Tlh1	Diaogoukou	Western	Catchment lhAI	River terrace	[60]
	Tlh2	Songshan 1	Central	Catchment lhAII	Marsh	[53]
	Tlh3	Songshan 2	Central	Catchment lhAII	Alluvial fan	[53]
	Tlh4	Hongjuanwan	Central	Catchment lhAII	River bank	[47]
	Tlh5	Woniushan	Central	Catchment lhAII	Mountain ridge	[47]
	Tlh6	Western amenxian	Central	Catchment lhB	River bank	[47]
	Tlh7	Eastern amenxian	Central	Catchment lhB	River bank	[61]
	Tlh8	Siniangniangmiao	Central	Catchment lhB	River terrace	[47]
	Tlh9	Shangeng	Central	Catchment lhC	River bank	[47, 61]
	Tlh10	Songshanshui	Central	Catchment lhC	River bank	[47, 61]
Haiyuan	Th1	Dashagou	Western	Catchment hA	River terrace	[62]
	Th2	Shenjiazhuang	Western	Catchment hA	River bank	[63]
	Th3	Huangliangtan	Western	Catchment hB	Alluvial fan	[64]
	Th4	Shaoshui	Central	Catchment hC	Alluvial fan	[64]
	Th5	Dayingshui	Central	Catchment hC	Bain	[65]
	Th6	Gaowanzi	Central	Catchment hDI	River terrace	[66, 67]
	Th7	Ganyanci 1	Eastern	Catchment hDII	Bain	[68]
	Th8	Ganyanci 2	Eastern	Catchment hDII	Bain	[68]
	Th9	Ganyanci 3	Eastern	Catchment hDII	Bain	[69]
	Th10	Shaojiazhuang 1	Eastern	Catchment hDIII	River terrace	[63]
	Th11	Shaojiazhuang 2	Eastern	Catchment hDIII	River terrace	[65]
	Th12	Shiqiaguangou	Eastern	Catchment hE	Sag pond	[70]
	Th13	Shaomayin	Eastern	Catchment hE	Sag pond	[71]
	Th14	Dagoumen	Eastern	Catchment hE	River terrace	[64]
	Th15	Caiyuan	Eastern	Catchment hE	River terrace	[71]
	Th16	Ciergou 1	Eastern	Catchment hE	River terrace	[64, 72]
	Th17	Ciergou 2	Eastern	Catchment hE	River bank	[73]
	Th18	Xiaoshandong	Eastern	Catchment hF	Alluvial fan	[65]
	Th19	Huanggaowan	Southeastern	Catchment hG	River terrace	[74]
	Th20	Shangdazhai	Southeastern	Catchment hH	River terrace	[74]
	Th21	Dazhiyao	Southeastern	Catchment hH	River terrace	[74]
	Th22	Sunjiahzuang	Southeastern	Catchment hI	River bank	[75]
	Th23	Houmohe	Southeastern	Catchment hI	River terrace	[75]

Note: — indicates that there are no named fault segments or that the geomorphic unit where the trench was excavated was not mentioned in the reference.

the trench wall. The dates were processed over a period spanning the 1980s to recent years. Different radiocarbon calibrations may result in differing ^{14}C dating results. To maintain consistency, we presented a consistent recalibration of all ^{14}C dating samples by using the OxCal program (version 4.4) and the IntCal20 curve [76] and presented the results in Table S1.

Using the above principles, single-trench columnar sedimentary sequences were obtained for all forty-four trenches (Figures 3–6). Trench Tm2 is composed of an upper soil layer and a lower slope deposit with a colluvial wedge between them [59]. However, there was a paleo erosion plane below the soil layer, and the only dating sample (with a dating result of 940 years B.P.) was collected in this soil layer. This draws the conclusion that the Maomaoshan fault has been inactive since 940 years B.P., which is consistent with the more precise dates from trench Tm1 but does not add any further age constraint. Hence, this trench was not considered in the event chronology.

Rupture barriers, which obstruct earthquake propagation, are commonly found in large-scale strike-slip fault systems [17, 23, 24, 77, 78]. Geometric discontinuities, such as large-scale fault steps and drastic fault strike changes, often characterize fault systems and provide a basis for structural segmentation [79, 80]. The Lenglongling, Maomaoshan, Laohushan, and Haiyuan faults can be separated into segments, based on the notable structural complexities and discontinuities of the surface traces [41, 43]. The Lenglongling fault consists of three segments according to a fault bend east of trench Tle1 and the fault intersection between trenches Tle4 and Tle5 (Figure 4(a)). A fault strike change of over 90° separates the Tianzhu Basin segment and the Longgou segment of the Maomaoshan fault (Figure 3(b)). The fault bifurcation between trenches Tlh1 and Tlh2 and a fault strike change east of trench Tlh10 split up the 3 segments of the Laohushan fault (Figure 5(a)). The Haiyuan fault also contains 4 segments that are bounded by the Shaoshui and Ganyanchi pull-apart basins and the drastic fault strike change between Th18 and Th19 (Figure 6(a)). Subsequently, we divided the trenches of different fault segments into different groups to establish multi-trench composite earthquake sequences.

The subsidiary faults of the Qilian-Haiyuan fault zone are mostly located along the mountain front with well-developed river systems (Figure 1). Paleoearthquake trenches are often excavated on river terraces or alluvial fans (Table 1), where Quaternary unconsolidated sediments are derived from snowmelt and fluvial erosion of nearby rivers. The sedimentary environment can significantly impact the formation and preservation of earthquake-derived sedimentary evidence. Compared with those of different drainage basins, less difference is shown within a given drainage basin in the source of sediment and response to climate change. There are differences in the sediment grain size at different geomorphological positions within a drainage basin; however, the priority of trench excavation is usually given to the areas with medium-fine sediments, such as where the river flows out of the mountain or the middle part of an alluvial fan. Trenches within the same drainage basin should have similar sedimentary environments; hence, we delineated drainage basins along 6 subsidiary faults to divide trenches with similar sedimentary environments into groups (Figures 3(a), 3(b), 4(a), 5(a) and 6(a)). Large rivers, including the Hei He, Datong He, Zhuanglang He, Gulang He, and the primary tributaries of the Yellow River (e.g., Sitandasha He and Qingshui He), are located near these faults. We considered the watersheds of the primary tributaries of these rivers covering the paleoearthquake trench as units to delimit the drainage basins and divide the trenches into different catchments. Consider the Lenglongling fault as an example (Figure 4(a)). The Liuhuang Gou (stream), Taola Gou, and Talihua Gou are the primary tributaries of the Datong He. We divided the six trenches along the Lenglongling fault into three catchments (leA to leC) based on the drainage basins of the Liuhuang Gou, Taola Gou, and Talihua Gou.

The catchments were separated to construct multitrench composite sedimentary sequences after trench grouping based on a combination of fault segmentation and drainage basin division. We used three main factors to correlate sedimentary units among multiple trenches: similar sedimentary characteristics (such as color and grain size), dated samples of similar ages, and similar trends of sedimentary characteristics over time. It is possible for sediments from the same period to appear as sedimentary units of varying thicknesses in different trenches owing to various sedimentation rates and erosion rates. In addition, it is common for different scholars to produce different assessments of lithology and stratification for a given set of sediments. We attempted to establish a reliable composite sedimentary sequence of multiple trenches by maintaining key sedimentary characteristics, using more detailed stratification, and preserving the unit thickness as much as possible (Figures 3–6).

To establish the age framework of each composite sedimentary sequence of the multiple trenches, we built deposition models of dating samples using the OxCal program (Figures 3–6). In the forty-three trenches, three dating methods were applied to date sedimentary units. These include the ^{14}C dating method, optically stimulated luminescence (OSL) dating method, and thermoluminescence (TL) dating method. Charcoal, organic sediment, peat, and wood are common sample types used in ^{14}C dating. In the case of conflicting ages, the priority for adopting the results from different dating methods is ^{14}C (charcoal, peat, and wood) $\geq$ ^{14}C (organic sediment) $\geq$ OSL > TL. The dating samples collected in the colluvial wedge and fault gouge were considered during the age framework determination. We considered these samples as dating data between two sedimentary units. A convincing age framework should be one that is supported by the majority of dating samples and reflects the main trend of the age variation with depth, in which the deeper sample must have a larger age. Consequently, we eliminated any outliers that were too old or too young, such as the gray dating samples shown in the composite sedimentary sequence of catchments leA, lhAI, hDI, and hDIII (Figures 4(b), 5(b), 6(e) and 6(g)). To prevent the effect

of a large inherited age, we are inclined to use the younger sample among those collected in the same sedimentation horizon. Besides, almost no paleo erosion plane or large-scale unconformity contact was observed in these trenches. We defined the unit thickness as the greatest thickness unit among multiple trenches during the establishment of the composite sedimentary sequence of multiple trenches. After minimizing the effect of long-term sedimentation disruptions and subsequent erosion, we attempted to simulate the possible long-term average sedimentation rates, represented by the dotted lines in the age framework diagrams in Figures 3–6. This was done by combining the composite sedimentary sequences of multiple trenches and their age framework.

3.3. Event Indicator Evaluation. An original and undisturbed sedimentary unit in a trench typically forms a horizontal layer of consistent or gradually varying thickness without reshaping by faulting. It is likely that the disruption and deformation of a sedimentary layer indicate a paleoearthquake and preserve its earthquake horizon, which is regarded as an event indicator. Common event indicators include colluvial wedges, sediments ponded against the scarps, material-filled fissures, vertical offset of a sedimentary unit, upward terminations of faults, sedimentary folding, angular unconformities, and so on [23, 81].

The quality of an event indicator is the most important factor for evaluating the probability of event occurrence [69, 82–84]. An event indicator that can only be produced by an earthquake is of high quality. We categorized colluvial wedges, sediments ponded against the scarps, and material-filled fissures as be the high-quality indicators. They are characterized not only by earthquake-derived intense deformation but also by distinctive earthquake-induced sediments near the fault between two ordinary sedimentary units. The colluvial wedge is the most frequently used indicator of reverse fault. A fault scarp emerges as the fault moves. During the degradation of this fault scarp, the erosion of the hanging wall provides colluvial debris that accumulates on the local footwall to form a colluvial wedge [85, 86]. Sag ponds are a type of offset geomorphology. After faulting, a flow is stopped by the newly dislocated footwall, and a sag pond forms in which fine-grained deposits record this earthquake [87, 88]. The initiation of sedimentation in the sag pond indicated the development of a fault scarp, which was caused by a strong earthquake. A material-filled fissure is derived from a coseismic fissure opening to the ground as a fault shakes. It is subsequently filled with younger out-of-sequence material [89, 90]. These three high-quality event indicators were used to identify the most likely earthquakes. However, there may be other nonearthquake causative mechanisms for low-quality indicators, which can only be used to identify possible events.

According to the bracketing sedimentary units recorded in previous studies, the events were matched to single-trench sedimentary sequences (Figures 3–6). The single-trench events were subdivided into two types depending on the quality of the event indicators: very likely earthquakes and possible earthquakes. Details of the single-trench event indicators are given in Table S2. The results revealed 73 very likely earthquakes and 76 possible earthquakes.

3.4. Event Constraints. The single-trench events were matched to multitrench composite sedimentary sequences (Figures 3–6) based on their sedimentary horizons in the single-trench sequences (Table S2). Very likely earthquakes identified by high-quality event indicators allow us to delineate reliable earthquake horizons. For instance, in catchment leC on the Lenglongling fault (Figure 4(d)), a reliable earthquake horizon was recognized between sedimentary units SleC3 and SleC4 by correlating two very likely earthquakes Ele5-2 and Ele6-3. This horizon represents the single-catchment event EleC3 and its occurrence time is constrained by the formation time of the units above and below. A good age constraint was derived from the oldest ^{14}C dating sample in the upper unit and the youngest ^{14}C dating sample in the lower unit. Following the same method, the occurrence timings of multitrench events can be determined by appropriate dating samples above and below their earthquake horizons (Figures 3–6). These earthquake horizons marked by very likely earthquakes have often appeared as very likely earthquakes or possible earthquakes in multiple trenches, particularly in catchments containing more than one trench along the Laohushan and Haiyuan faults. In addition, we found that some sedimentary horizons were supported by more than one possible earthquake (without a very likely earthquake) in catchments leB and leC on the Lenglongling fault and catchments hC and hH on the Haiyuan fault (Figures 4(c), 4(d), 6(d) and 6(k)). They are very likely to reveal earthquake horizons. For instance, two possible earthquakes (Ele5-1 and Ele6-1) appear between units SleC1 and SleC2 in catchment leC on the Lenglongling fault (Figure 4(d)). Although their event indicators were of lower quality, they were both identified by multiple event indicators (Table S2). We considered that these two possible earthquakes are likely to reveal an earthquake horizon and represent the single-catchment event EleC1 with an upper age bound from the dating result of unit SleC2.

Only one catchment was defined for the Tuolaishan, Jinqianghe, and Maomaoshan faults due to a small number of trenches with uneven distributions (Figure 3). Along these three faults, we assumed that single-catchment events are single-fault events. The single-catchment events were integrated to constrain single-fault events on faults with more defined catchments, such as the Lenglongling, Laohushan, and Haiyuan faults (Figure 7). The time window common to all the different ages of the single-catchment events should be the most likely age for this single-fault event [25, 91]. Considering the uncertainties of sediment dating and single-catchment event age constraints, we regard two single-catchment events whose ages have a difference of less than 300 years as the same single-fault event [54, 68] unless there are two determined seismic events marked in one catchment. For instance, although the age intervals of events EleA1 and EleC3 did not overlap, these two events were of similar age and both

occurred after the deposition of peat layers (Figure 4). It is likely that they represent the same event (Figure 7(a)). In some cases, there is only an upper or lower age bound for a single-catchment event due to insufficient dating samples. In such cases, this event was generally proposed to represent the same single-fault event of the closest age that has been constrained by other single-catchment events. For instance, event ElhC1 on the Laohushan fault has a lower age bound determined by a dating sample at the bottom of its upper unit without an upper age bound (Figure 5(e)). It occurred before 4180 years B.P.; hence, we assumed that it represents the same event as ElhAI2 (Figure 7(d)).

In the meantime, the principles of the maximum rupture model were followed to estimate the rupture extent [92]. The maximum rupture model accommodates all the events with the fewest possible ruptures to determine the rupture length along the strike. In the basic consideration of fault geometric segmentation, our model regarded one catchment as a spatial unit during the estimation of rupture extent. If single-catchment events in the two catchments fit in time, the rupture would be extended; otherwise, the rupture would cease on the boundary of the catchment. Combined, the occurrence timings of single-fault events and the fault sections they ruptured were constrained (shown as light blue bars in Figures 7(b), 7(d), and 7(f)) on the Lenglongling, Laohushan, and Haiyuan faults.

The age intervals of some single-fault events remain wide after the preliminary age limitation, some up to 2000 years. We propose considering the relationship between dated horizons and earthquake horizons to improve age constraints. Scenario 1: A large age interval is controlled by the long distance between the earthquake horizons and their upper or lower dating samples, or there is no upper dating sample but the present timing to supply a limitation of the lower age bound of the youngest event. In these cases, we improved the event ages by using the distance between the dated and earthquake horizons with the estimated long-term sedimentation rate to reduce the event age interval to within 600 years. Scenario 2: A given event has only the upper (or lower) age bound, which is derived from a dating sample at the top (bottom) of the lower (upper) unit. Therefore, it is likely that the event occurred close in time to the dating sample. Scenario 3: A colluvial wedge generally forms later than, but very close to, the earthquake occurrence. If a dating sample is collected in the central part of the colluvial wedge close to the pre-post event transition zone [93], we suggest that the age of the event age can be estimated to be within 300 years prior to the dating result. Additionally, colluvial wedges are more reliable than the sedimentary units above and below an earthquake horizon. If all three scenarios appear simultaneously, we prioritized the age of the colluvial wedge (Scenario 3) when combining multiple single-catchment events to determine the age of a single-fault event. Thus, the age constraint of single-fault events improved (Table S3). As a result, the age intervals (shown as the dark blue bars in Figures 7(d) and 7(f)), except that of the oldest event Eh10 that occurred before 10 ka, can be narrowed to within 300 or 600 years.

4. Results

Only one event (Event Et1) was discovered on the Tuolaishan fault and occurred between 4050 and 3840 years B.P., rupturing at least the fault section in catchment tA (Figure 8(b)). Seven events were constrained on the Lenglongling fault. These are events Ele7 to Ele1 with occurrence timings ranging from 8410–8030, 7940–7660, 7290–7145, 5900–5600, 3890–3400, and 2880–2310 to <550 years B.P. The extent of their ruptures is depicted in Figures 7(b) and 8(b). Event Ej3 was the sole event found on the Jinqianghe fault, occurring between 4000 and 3700 years B.P. with a minimum rupture of the Jinqianghe segment in catchment jA (Figure 3(d) and Table S3 Table S3). An event was also found on the Maomaoshan fault, event Em1, which occurred between 2500 and 1900 years B.P. and caused at least the rupture of the fault section of the Tianzhu Basin segment in catchment mA (Table S3 and Figure 8(b)). On the Laohushan fault, six paleoearthquakes (events Elh6 to Elh1) were found to occur at dates >>7750, 6440–6140, 6000–5200, 4115–3610, 1540–1350, and <320 years B.P. The rupture extents of these events are shown as blue bars in Figures 7(d) and 8(b). Ten paleoearthquakes were constrained on the Haiyuan fault, Eh10 to Eh1, with occurrence timings ranging from 12850–11870, 9000–8690, 8280–7820, 5930–5910, 4690–4410, 3020–2840, 2125–1925, 980–650, 155–140 years B.P. to 1920 A.D. The fault sections ruptured during these earthquakes are displayed in Figures 7(f) and 8(b).

5. Discussion

5.1. Conditional Rupture Barriers and Earthquake Behaviors on the Subsidiary Faults. The events reconstrained by this study are those identified through high-quality or multitrench lower-quality event indicators. After this strict qualification, the probability of those events being true earthquakes and strong earthquakes ($M \geq 7$) with heavy damage should be very high. Multitrench sedimentary sequences are constructed to provide more precise constraints on when those strong earthquakes occurred. The event ages were estimated more accurately by integrating the limited number of dating samples in each single trench, followed by and refining the age constraints of multicatchment events based on the stratigraphic relationship between earthquake horizons and the dated samples. The division of the subsidiary faults into smaller, more manageable units through a combination of fault segmentation and watershed delineation allow for the creation of the sedimentary sequences and refinement of multitrench event constraints. This process allowed us to refine the determination of the maximum possible along-strike rupture extents of the strong events identified here and further study the probable rupture segmentation along the subsidiary faults.

The seven events identified on the Lenglongling fault follow a quasiperiodic recurrence pattern. If we group events Ele7 to Ele5 as an earthquake cluster that spanned approximately a thousand years, the reoccurrence periodicity of events Ele5 to Ele1 is stronger, with an

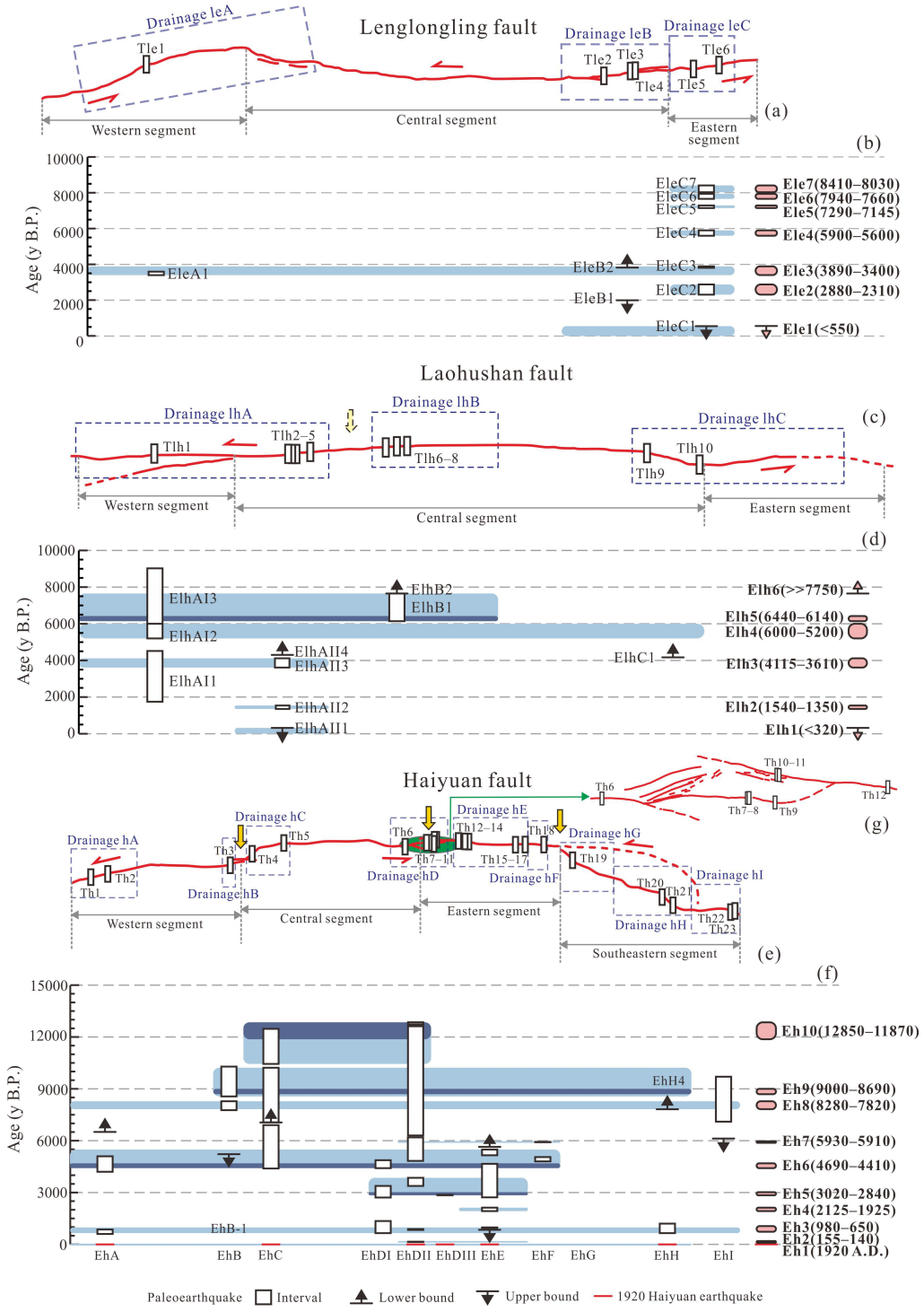

FIGURE 7: Age constraint of paleoearthquakes on the Lenglongling, Laohushan, and Haiyuan faults. Distribution maps of the (a) Lenglongling, (c) Laohushan, and (e) Haiyuan faults are depicted including the trenches, fault segments, and drainage basins. Dash light yellow arrow between trenches Tlh6 and Tlh7 shows a possible false-positive rupture barrier of the Laohushan fault. Yellow arrows along the Haiyuan fault represent the rupture segmentation boundaries that are inferred from the rupture extents of paleoearthquakes. Space-time diagrams of paleoearthquakes are displayed on the (b) Lenglongling, (d) Laohushan, and (f) Haiyuan faults, respectively. The white boxes mark single-catchment events, while the light blue bars indicate the preliminary age constraint of single-fault events and the fault sections ruptured. The dark blue bars show the improved limitation of occurrence timings of the single-fault events. The pink boxes represent the compilation of all paleoearthquakes on the subsidiary fault. (g) The distribution map of fault traces and trenches in the Ganyanchi pull-apart basin.

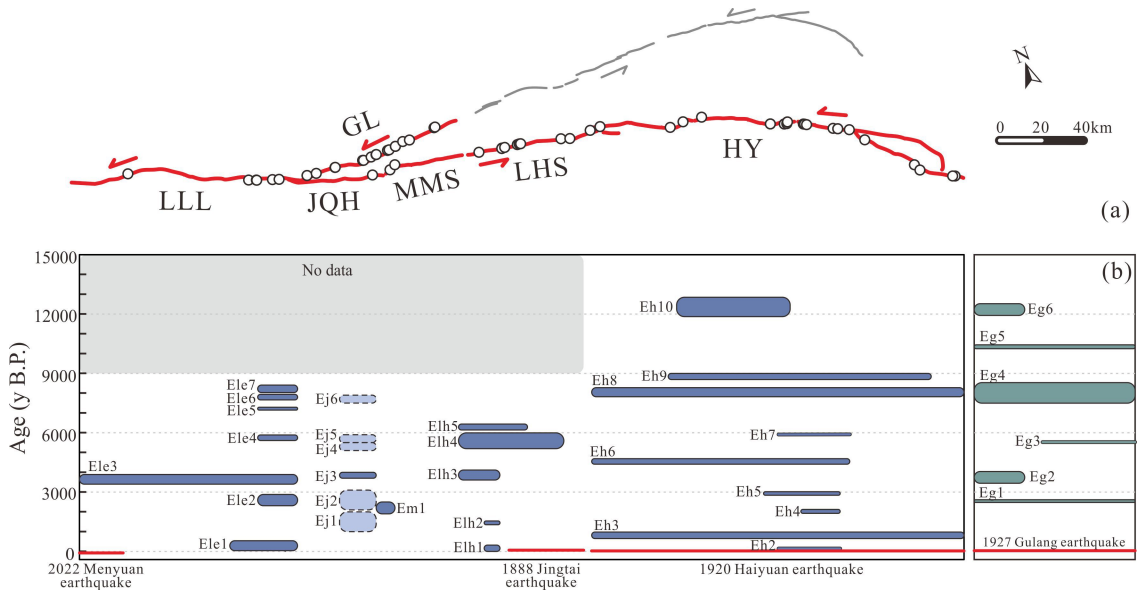

FIGURE 8: (a) Map of the central–eastern Qilian–Haiyuan fault zone and the Gulang fault (red lines). The paleoearthquake trenches are represented by black circles. (b) The occurrence timings and rupture extents of the paleoearthquakes (bars) and historical earthquakes (red lines) on the central–eastern Qilian–Haiyuan fault zone (blue bars) and the Gulang fault (green bars). The light blue bars surrounded by the dashed lines are the events identified by clustered geomorphic offsets along the Jinqianghe fault in Reference 29. Fault abbreviations: LLL = Lenglongling fault; JQH = Jinqianghe fault; MMS = Maomaoshan fault; LHS = Laohushan fault; HY = Haiyuan fault; GL = Gulang fault.

average reoccurrence interval of approximately 1770 years. However, as five out of six trenches along the Lenglongling fault are located at its eastern end (Figure 7(a)), it is challenging to identify a clean pattern of rupture segmentation on the fault.

On the Laohushan fault, there is likely a false-positive rupture barrier between the catchments lhA and lhB, indicated by the dashed yellow arrow in Figure 7(c). This barrier appears to impact the rupture of events Elh3, Elh2, and Elh1. However, the trenches in catchments lhB and lhC do not have the finely layered young sedimentary units that are available in catchment lhA; therefore, it is unknown whether younger events induced rupture in these areas. The earthquakes on this fault also display a quasiperiodic pattern of recurrence, with an average interval of approximately 1660 years for events Elh5 to Elh1.

On the Haiyuan fault, the occurrence of events Eh10 to Eh1 (Figure 7(f)) was substantially periodic, with an average interval of approximately 1370 years. Based on the analysis of sedimentary sequences in different catchments and typical single-fault events, three potential barriers may exist (yellow arrows in Figure 7(e)) on this fault. The western one is located between catchments hB and hC and is likely to have been formed by the Shaoshui pull-apart basin. The ruptures of events Eh10 and Eh9 were affected by this barrier and stopped on two sides of the Shaoshui Basin. The central one is within catchment hDII, which correlates spatially with another pull-apart basin, the Ganyanchi Basin. It stopped the ruptures of events Eh10, Eh7, Eh5, and Eh2 on the boundaries of the basin. As a new fault crossing the Ganyanchi basin forms, two basin-bounding faults have been linked [68, 94, 95]. To analyze the earthquake occurrence of the cross-basin fault and the two fault sections located to the west and east of the basin, the trenches in catchment hD were divided into three groups, catchments hDI, hDII, and hDIII (Figures 6(e–g) and 7(g)). The event constraining result validates that the cross-basin fault inside the Ganyanchi pull-apart basin has always ruptured together with two fault sections west and east of the basin (but not necessarily with both sides at once) since 15 ka. This observation may indicate that the Ganyanchi–Shaojiazhuang cross-basin fault gradually took the place of the basin-bounding faults and become a major contributor to the strong earthquakes. The eastern rupture barrier exists between catchments hF and hG, showing a good correlation with the dramatic change (approximately 20°–25°) of the fault strike between the middle and eastern segments of the Haiyuan fault. The ruptures of events Eh10, Eh7, Eh4, and Eh2 are impeded by this barrier. Sometimes, the rupture breaks through the barrier to reach other segments divided by rupture barriers, such as event Eh5. These barriers are similar to those of broader barrier zones. The cessation of the rupture was associated with the release of energy during the earthquake and the rupture of the fault. Some rupture terminations may have been due to missing geologic records for some trenches, but others are more ones that can be defensible due to good sedimentary completeness in neighboring catchments. Paleoseismic trenches on a fault can provide a good constraint on rupture events and their rupture lengths when the trenches have an appropriate distribution and sufficient quantity.

Rupture barriers that affect the rupture propagation of paleoearthquakes are generally associated with the geometric discontinuities of the fault [79, 80, 96–99].

Different rupture segments may have different slip behaviors, which are shown in the slip rate, cumulative offset distribution, and the patterns of earthquake occurrence. The rupture barriers discovered within the Haiyuan faults are all conditional rupture barriers [100, 101], terminating some ruptures but allowing other earthquakes to pass. The magnitude and rupture direction of a given earthquake, and the size and stability of the barrier, work in concert to influence whether a rupture passes the rupture barrier.

5.2. Earthquake Cycles Traversing the Central–Eastern Qilian–Haiyuan Fault Zone. Liang et al. [102] constrained the paleoearthquakes of the Gulang fault by establishing sedimentary sequences of different catchments. In this study, we further improved the Gulang fault earthquake age constraints by considering the relationship between earthquake horizons and dated horizons in multitrench sedimentary sequences, using the method detailed in section 3.4 (Table S3). Thus, the timing of the occurrence of six paleoearthquakes on the Gulang fault, events Eg6 to Eg1, was re-estimated to be 12500–11900, 10400–10200, 8470–7420, 5450–5410, 3930–3330, and 2490–2350 years B.P., respectively (Figure 8(b)).

Alternatively, the Jinqianghe Fault is located in natural reserves, making trench excavation challenging. There is only one trench on the Jinqianghe fault, and it is common for a single trench to miss paleoearthquakes [17, 26, 98]. The construction of cumulative offset clusters is effective at unveiling the earthquake history of active faults [103–106]. To understand the long-term seismic history of the Jinqianghe fault, we combined the prehistorical earthquakes constrained by this study with those revealed by the cumulative offset clusters of this fault [29]. Six events (events Ej6 to Ej1) can be found with occurrence timings of 7900–7500, 5900–5500, 5500–5100, 4000–3700, 3100–2100, and 2000–1000 years B.P. and the minimum ruptures, including the Jinqianghe segment in catchment jA (Figure 8(b)). Notably, the events obtained from offset clusters have higher uncertainty compared with those recorded in trenches.

The relative motions of the Alxa, Ordos, and Qaidam blocks make the Qilian–Haiyuan fault zone and its surrounding regions the primary areas of earthquake occurrence in the northeastern Tibetan Plateau. We reconstructed the spatiotemporal distribution of strong earthquakes to capture the reoccurrence behavior of the central–eastern Qilian–Haiyuan fault zone and Gulang fault. Strong historical earthquakes with ground surface ruptures have occurred on these faults, including the Jingtai earthquake in 1888, the Haiyuan earthquake in 1920, the Gulang earthquake in 1927, and the Menyuan earthquake in 2022 (Figure 1) [31, 47, 49, 50, 107]. The fault that caused the Gulang earthquake in 1927 remains a question of debate. The Gulang earthquake is thought by some to have caused the rupture of the entire Gulang fault [107, 108], whereas [56] argued that it was generated by the slip of both the Lenglongling fault and the southern fault of the Wuwei Basin. The field-geology survey shows that the surface rupture zone along the Lenglongling fault should be the product of an older historical earthquake instead of the 1927 Gulang earthquake. Event Ele1 is the latest event discovered in the trenches of the Lenglongling fault. He et al. [57] inferred that event Ele1 was a strong earthquake that occurred in the central-western part of Gansu province in 1540 A.D.. Our belief is that the surface rupture zone along the Lenglongling fault was the result of the 1540 historical earthquake, while the 1927 Gulang earthquake caused the rupture of the Gulang fault.

The frequency of earthquakes over time was calculated using the cumulative probability distribution (CPD) formula and kernel density analysis. The bandwidth for the analysis was set at 336 years, which is the average reoccurrence interval of all strong paleoearthquakes and historical earthquakes. The magnitude of each paleoearthquake was estimated based on the empirical relationship between the magnitude and surface rupture length of strike-slip faults [109]. The earthquake magnitudes derived from this study were categorized as $M = 7.0$ for $M \leq 7.0$, $M = 7.5$ for $7.0 < M \leq 7.5$, and $M = 8.0$ for $7.5 < M \leq 8.0$ in Figure 9(a).

Seven CPD peaks can be observed in Figure 9a. The two earliest peaks, resulting from the three paleoearthquakes on the Haiyuan and Gulang faults, were not robust enough to establish clustered behavior prior to 10 ka. Five more recent peaks, with ample data, allowed for the identification of five earthquake clusters, designated as clusters C1–C5. These five clusters spanned 8845–7218, 6290–5300, 4550–3630, 2930–1445, and 815 years B.P. to present, respectively (Table S4). The durations of clusters C2, C3, and C5 were ~900–1000 years, while those of clusters C1 and C4 were ~1500–1600 years. The Haiyuan fault ruptured first among the majority of earthquake clusters, and this rupture occurred far ahead of the main earthquake group. Furthermore, after mapping extent of the rupture according to the chronological order of events (Figure 9b), it was revealed that the earthquakes tended to migrate gradually from the eastern toward the central Qilian–Haiyuan fault zone. We identified a total of seven migrations, Mg1–Mg7, spanning 8845–8220, 8050–7218, 6290–5300, 4550–3630, 2930–2200, 2025–1445, and 815 years B.P. to present (Table S4). The average duration was approximately 800 years. Earthquake migration usually begins with the rupture of the Haiyuan fault. Furthermore, each earthquake cluster included one or two earthquake migrations. Thus, these seven earthquake migrations represent temporally clustered behavior with two types of intermigration periods. One type of intermigration period is 600–900 years (between clusters), while the other is much shorter, about 170 years (within a cluster). The intermigration periods between Mg1 and Mg2 and between Mg5 and Mg6 are shorter and fall under the latter type. The initial rupture of the Haiyuan fault frequently triggered the formation of these earthquake clusters and migrations. Similar to the first domino, it might trigger nearby earthquakes by changing the Coulomb stress and further promoting the formation of temporal clusters and spatial migrations of strong earthquakes in this region.

The latest migration, Mg7, may be incomplete. There remains a seismic gap in the central Qilian–Haiyuan fault

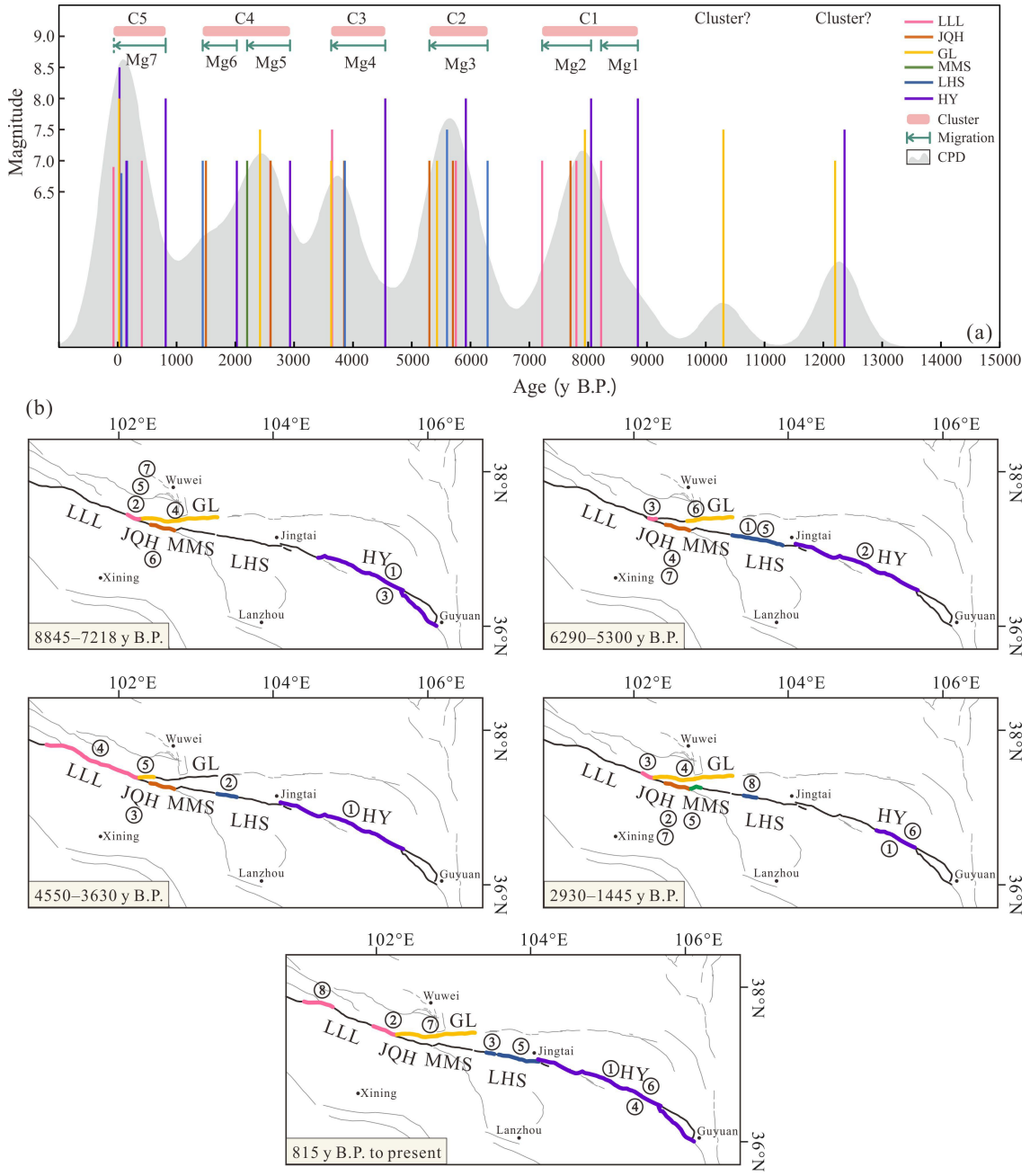

FIGURE 9: (a) Earthquake clusters and earthquake migrations traversing the central–eastern Qilian–Haiyuan fault zone. The dashed line on the left of the green lines depicting migration Mg7 means that this latest earthquake migration may not be complete. (b) The rupture distribution of the strong earthquakes shown in Table S4 in the earthquake clusters traversing the central–eastern Qilian–Haiyuan fault zone, including clusters C1 (8845 and 7218 years B.P.), C2 (6290 and 5300 years B.P), C3 (4550 and 3630 years B.P.), C4 (2930 and 1445 years B.P.), and C5 (815 years B.P. to present). The colored lines outline the rupture extents with the order of event occurrence indicated by the numbers in black circles. There have been little seismic data on the Maomaoshan fault so far; it is unknown whether it ruptured in these past sequences except for event Em1.

zone, which consists of the Jinqianghe fault, Maomaoshan fault, and the central part of the Lenglongling fault (Figure 9(b)). This gap is termed the "Tianzhu seismic gap" [110–112]. This strain accumulation zone [113, 114] is potentially a high seismic hazard for earthquakes with $M \geq 7$; in recent years, moderate earthquakes have frequently occurred in the region. Unfortunately, the understanding of the reoccurrence behavior of strong earthquakes in the Qilian–Haiyuan fault zone is limited by the scarce data obtained from trenching research on the Tuolaishan and Maomaoshan faults. Further data collection is necessary to provide a more comprehensive understanding of seismic activity in this region.

5.3. Reoccurrence Patterns of Strong Earthquakes in the Block-Boundary Fault Zone. Temporal clusters and spatial

migrations of strong earthquakes commonly occur in plate-boundary fault zones, such as the North Anatolian fault, and the San Andreas fault system, and these are associated with earthquake triggering [115–120]. Furthermore, earthquake triggering between faults and fault segments is a common phenomenon in the fault zones between intraplate active blocks of mainland China. Four successive $M > 6$ earthquakes between 1973 and 1982 were influenced by Coulomb stress change related to fault interactions in the Xianshuihe fault zone [121, 122]. On the Longmenshan fault, the 2013 Lushan earthquake in the southern section was induced by the inelastic triggering of the 2008 Wenchuan earthquake in the north-central section [123]. Within a large-scale block-boundary fault zone spanning hundreds of kilometers, the preparation and occurrence of strong earthquakes do not proceed independently on a single fault but are largely influenced by fault interactions, likely via Coulomb stress transfer. Consequently, the construction of the earthquake rupture chronology and the forecasting of future strong earthquakes should be carried out by considering a fault zone in its entirety rather than by considering a single subsidiary fault inside it.

6. Conclusions

Block-boundary fault zones, composed of multiple interacting subsidiary faults, are the primary sources of strong earthquakes in continental environments. The earthquake history of these large-scale fault zones provides a valuable case for understanding the long-term repeated behavior of strong earthquakes.

The Qilian–Haiyuan fault zone locates in the Alxa, Qaidam, and Ordos blocks have been taken used to enhance the multitrench constraining method through the development of sedimentary sequences of the trenches that are grouped into different drainage basins. This study revealed a series of strong paleoearthquakes on six subsidiary faults and provided improved constraints on the ages and extents of these events. Analysis of the ruptured fault sections during these prehistoric earthquakes led to the identification of three conditional rupture barriers that could be identified on the Haiyuan fault, which are associated with the significant along-fault geometric discontinuities. The results also highlight regular patterns of reoccurrence of earthquakes on subsidiary faults, as summarized from the paleoearthquake sequences.

Finally, this study, combined with previous research and data on ground-rupturing historical earthquakes, enabled the determination of the spatial and temporal distributions of strong earthquakes within the central–eastern Qilian–Haiyuan fault zone. This analysis revealed the presence of five earthquake clusters since 10 ka. These clusters were dated to occur between 8845 and 7218, 6290 and 5300, 4550 and 3630, 2930 and 1445, and 815 years B.P. to present. The events exhibited a migratory pattern, typically moving from the eastern to the central portion of the Qilian–Haiyuan fault zone, forming seven earthquake migrations that lasted an average of approximately 800 years each. The latest migration (Mg7) may not yet have been completed, as a seismic gap remains, indicating a high likelihood of a future $M \geq 7$ earthquake in this area.

Conclusively, earthquake triggering is a widely observed phenomenon between adjacent faults within a large-scale block-boundary fault zone, highlighting the importance of considering fault interactions in the study of earthquake cycles and seismic hazard analysis.

Data Availability

The original contributions presented in this study are included in the article and the supplementary data, further inquiries can be directed to the corresponding author. The topographic base map of Figures 1–6 was generated from 30 m resolution Advanced Spaceborne Thermal Emission and Reflection Radiometer (ASTER) Global Digital Elevation Map (GDEM) data downloaded from the National Aeronautics and Space Administration (https://asterweb.jpl.nasa.gov/gdem.asp/).

Conflicts of Interest

The authors declare no conflicts of interest.

Acknowledgments

This work was supported by the National Key Research and Development Program of China (no. 2017YFC1500100), the second Tibetan Plateau Scientific Expedition and Research Program (STEP) (no. 2019QZKK0901), and the National Science Foundation of China (nos. 42174062 and 41774049). We also express our thanks to Xiaohui He and Chuang Sun for their valuable discussions.

Supplementary Materials

The supplementary data includes the following: (1) Recalibration of the ^{14}C dating samples in trenches (Table S1); (2) Sedimentary horizons, event indicators, and occurrence probabilities of the single-trench events (Table S2); (3) Improvement of age constraint of the single-fault events (Table S3); (4) Clusters and migrations of strong events surrounding the central–eastern Qilian–Haiyuan fault zone (Table S4).

References

[1] R. E. Wallace, "Grouping and migration of surface Faulting and variation in slip rates on faults in the great Basin province," *Bulletin of the Seismological Society of America*, vol. 77, pp. 868–887, 1987.

[2] Y. Y. Kagan and D. D. Jackson, "Long-Tern earthquake clustering," *Geophysical Journal International*, vol. 104, no. 1, pp. 117–134, 1991. http://blackwell-synergy.com/doi/abs/10.1111/gji.1991.104.issue-1.

[3] R. S. Stein, A. A. Barka, and J. H. Dieterich, "Progressive failure on the North Anatolian fault since 1939 by earthquake stress triggering," *Geophysical Journal International*,

vol. 128, no. 3, pp. 594–604, 1997. http://blackwell-synergy.com/doi/abs/10.1111/gji.1997.128.issue-3.

[4] S. Das and C. H. Scholz, "Off-fault aftershock clusters caused by shear stress increase?," *Bulletin of the Seismological Society of America*, vol. 71, no. 5, pp. 1669–1675, 1981.

[5] G. C. P. King, R. S. Stein, and J. Lin, "Static stress changes and the triggering of earthquakes," *Bulletin of the Seismological Society of America*, vol. 84, pp. 935–953, 1994.

[6] R. A. Harris and R. W. Simpson, "Suppression of large earthquakes by stress shadows: A comparison of Coulomb and rate-and-state failure," *Journal of Geophysical Research*, vol. 103, no. B10, pp. 24439–24451, 1998.

[7] R. S. Stein, "The role of stress transfer in earthquake occurence," *Nature*, vol. 402, no. 6762, pp. 605–609, 1999.

[8] G. C. P. King and M. Cocco, "Fault interaction by elastic stress changes: New clues from earthquake sequences," *Advances in Geophysics*, vol. 44, pp. 1–36, 2000.

[9] J. Ma, "Changing viewpoint from fault to block: A discussion about the role of active block in Seismicity," *Earth Science Frontiers*, vol. 6, no. 4, pp. 363–370, 1999.

[10] J. Ma, "Tectonophysical research on fault block Tectonics and earthquakes," *Chinese Journal of Geology*, vol. 44, no. 4, pp. 1071–1082, 2009.

[11] P. Z. Zhang, "Late Quaternary tectonic deformation and earthquake hazard in continental China," *Quaternary Sciences*, vol. 39, no. 5, pp. 404–413, 1999.

[12] G. M. Zhang and P. Z. Zhang, "Academic progress on the mechanism and forecast for continental strong earthquake in the first two years," *China Basic Science*, vol. 2, no. 10, pp. 4–10, 2000.

[13] G. M. Zhang, H. S. Ma, H. Wang, and L. Li, "Relationship between the active blocks in Chinese mainland and the strong seismic activity," *Science in China (Series D)*, vol. 34, no. 7, pp. 591–599, 2004.

[14] G. M. Zhang, H. S. Ma, H. Wang, and X. L. Wang, "Boundaries between active-Tectonic blocks and strong earthquakes in China mainland," *Chinese Journal of Geophysics*, vol. 48, no. 3, pp. 662–671, 2005.

[15] P. Z. Zhang, Q. D. Deng, G. M. Zhang, et al., "Active tectonics blocks and strong earthquakes in the continent of China," *Science in China (Series D)*, vol. 33, no. S1, pp. 12–20, 2003.

[16] P. Z. Zhang, Q. D. Deng, Z. Q. Zhang, and H. B. Li, "Active faults, earthquake hazards and associated geodynamic processes in continental China," *Science in China (Series D)*, vol. 43, no. 10, pp. 1607–1620, 2013.

[17] D. P. Schwartz and K. J. Coppersmith, "Fault behavior and characteristic earthquakes: Examples from the Wasatch and San Andreas fault zones," *Journal of Geophysical Research*, vol. 89, no. B7, pp. 5681–5698, 1984.

[18] R. J. Weldon, T. E. Fumal, T. J. Powers, S. K. Pezzopane, K. M. Scharer, and J. C. Hamilton, "Structure and earthquake offsets on the San Andreas fault at the Wrightwood, California, Paleoseismic site," *Bulletin of the Seismological Society of America*, vol. 92, no. 7, pp. 2704–2725, 2002.

[19] J. Liu-Zeng, Y. Klinger, K. Sieh, C. Rubin, and G. Seitz, "Serial ruptures of the San Andreas fault, Carrizo plain, California, revealed by three-dimensional excavations," *Journal of Geophysical Research*, vol. 111, no. B2, p. n, 2006.

[20] K. R. Berryman, U. A. Cochran, K. J. Clark, G. P. Biasi, R. M. Langridge, and P. Villamor, "Major earthquakes occur regularly on an isolated plate boundary fault," *Science*, vol. 336, no. 6089, pp. 1690–1693, 2012.

[21] H. Peng, D. Zhang, W. Zheng, et al., "Recurrence and clustering of large earthquakes along the northern boundary of Ordos block: Constraining Paleoearthquakes by an improved multiple trench constraining method," *Lithosphere*, vol. 2022, no. 1, 2022.

[22] K. E. Sieh, "Prehistoric large earthquakes produced by slip on the San Andreas fault at Pallett Creek, California," *Journal of Geophysical Research*, vol. 83, no. B8, p. 3907, 1978.

[23] J. P. McCalpin, *"Paleoseismology (Second Edition),"* Academic Press, Oxford, UK, 2009.

[24] D. W. Burbank and R. S. Anderson, *"Tectonic Geomorphology (Second Edition),"* Blackwell Publishing, Chichester, 2012.

[25] J. P. McCalpin, "Spatial and temporal analysis of 1200 landslides in a 900 Km2 area, middle rocky mountains," *U.S. Geological Survey Open-File Report*, vol. 87–673, pp. 102–114, 1987.

[26] F. Y. Mao and P. Z. Zhang, "Progressive constraining method in paleoseismic study and paleoearthquakes along the major active faults in northern Xinjiang," in *Research on Active Fault*, 4:Institute of Geology, China Earthquake Administration, Eds, pp. 153–164, Institute of Geology, China Earthquake Administration, Seismological Press, Beijing, 1995.

[27] G. K. Yin and Q. L. Chen, "Characteristic index and statistical model of sediment yield in small drainage basins of Loess plateau in China," *Acta Geographica Sinica*, vol. 44, no. 1, pp. 32–46, 1989.

[28] S. P. Rice, "The nature and controls of downstream fining within sedimentary links," *Journal of Sedimentary Research*, vol. 69, no. 1, pp. 32–39, 1999.

[29] S. Liang, W. Zheng, G. Chen, et al, "Late Quaternary slip behavior of the Jinqianghe fault in the middle Qilian-Haiyuan fault zone, northeastern Tibetan plateau," *Acta Geologica Sinica (English Edition)*, vol. 96, no. 3, pp. 825–843, 2022.

[30] W. J. Zheng, Q. L. Wang, D. Y. Yuan, D. L. Zhang, Z. Q. Zhang, and Y. P. Zhang, "The concept, review and new insights of the active-tectonic block hypothesis," *Seismology and Geology*, vol. 42, no. 2, pp. 245–270, 2020.

[31] LIS (Lanzhou Institute of Seismology), and NSBC (Ningxia Seismological Bureau of China), *"The Great Haiyuan Earthquake in 1920,"* Seismological Press, Beijing, 1980.

[32] D. Qidong, F. Sung, S. Zhu, et al., "Active faulting and tectonics of the Ningxia-Hui autonomous region, China," *Journal of Geophysical Research*, vol. 89, no. B6, pp. 4427–4445, 1984.

[33] Q. D. Deng, S. F. Chen, F. M. Song, et al., "Variations in the geometry and amount of slip on the Haiyuan (Nanxihaushan) fault zone, China and the surface rupture of the 1920 Haiyuan earthquake," *Earthquake Source Mechanics*, vol. 37, pp. 169–182, 1986.

[34] G. Gu, T. Lin, and Z. Shi, *"Catalogue of Chinese Earthquakes (1881Bc-1969Ad),"* Science Press, Beijing, 1989.

[35] B. C. Burchfiel, P. Z. Zhang, Y. P. Wang, et al., "Geology of the Haiyuan fault zone, Ningxia-Hui autonomous region, China, and its relation to the evolution of the Northeastern margin of the Tibetan plateau," *Tectonics*, vol. 10, no. 6, pp. 1091–1110, 1991.

[36] K. M. Hou, Q. D. Deng, and B. C. Liu, "Research on tectonic environment and Seismogenic mechanism of 1927 Gulang great earthquake," *Earthquake Research in China*, vol. 15, no. 4, pp. 339–348, 1999.

[37] Z. X. Fu, G. P. Liu, and Q. F. Chen, "Dynamic analysis on interaction between the Haiyuan-Gulang-Changma great earthquake in the North boundary of the tibetan plateau," *Seismology and Geology*, vol. 23, no. 1, pp. 35–42, 2001.

[38] W. J. Zheng, D. Y. Yuan, P. Z. Zhang, et al., "Tectonic geometry and kinematic dissipation of the active faults in the Northeastern Tibet plateau and their implications for understanding Northeastward growth of the plateau," *Quaternary Research*, vol. 36, no. 4, pp. 775–788, 2016.

[39] A. R. Duvall, M. K. Clark, B. A. van der Pluijm, and C. Li, "Direct dating of Eocene reverse faulting in northeastern Tibet using Ar-dating of fault clays and low-temperature thermochronometry," *Earth and Planetary Science Letters*, vol. 304, nos. 3–4, pp. 520–526, 2011.

[40] R. O. Lease, D. W. Burbank, M. K. Clark, K. A. Farley, D. W. Zheng, and H. P. Zhang, "Middle Miocene reorganization of deformation along the Northeastern Tibetan plateau," *Geology*, vol. 39, no. 4, pp. 359–362, 2011.

[41] D. Yuan, W. Ge, Z. Chen, et al., "The growth of northeastern Tibet and its relevance to Large-Scale Continental Geodynamics: A review of recent studies," *Tectonics*, vol. 32, no. 5, pp. 1358–1370, 2013. https://onlinelibrary.wiley.com/toc/19449194/32/5.

[42] J. X. Yu, J. Z. Pang, Y. Z. Wang, et al., "Mid-Miocene uplift of the northern Qilian shan as a result of the northward growth of the northern Tibetan plateau," *Geosphere*, vol. 15, no. 2, pp. 423–432, 2019.

[43] W. Zheng, P. Zhang, W. He, et al., "Transformation of displacement between strike-slip and crustal shortening in the northern margin of the Tibetan plateau: Evidence from Decadal GPS measurements and late Quaternary slip rates on faults," *Tectonophysics*, vol. 584, January, pp. 267–280, 2013.

[44] D. Y. Yuan, "Tectonic deformation features and space-time evolution in northeastern margin of the Qinghai-Tibetan plateau since the late Cenozoic time (Doctor thesis)," in *Institute of Geology*, China Earthquake Administrator, Beijing, 2003.

[45] T. Chen, J. Liu-Zeng, Y. X. Shao, et al., "Geomorphic offsets along the creeping Laohu shan section of the Haiyuan fault, northern Tibetan plateau," *Geosphere*, vol. 14, no. 3, pp. 1165–1186, 2018.

[46] J. R. Liu, Z. K. Ren, H. P. Zhang, et al., "Slip rates along the Laohushan fault and spatial variation in slip rate along the Haiyuan fault zone," *Tectonics*, vol. 41, no. 2, 2022.

[47] D. Y. Yuan, B. C. Liu, T. Y. Lu, et al, "Research on Paleoearthquake along the Laohushan active fault zone, " in *Research on Active Fault*, 2: Institute of Geology, China Earthquake Administration, Eds, pp. 160–169, Seismological Press, Beijing, 1994.

[48] Q. D. Deng, "Learning and progressing through scientific practices: commemorating the 90th anniversary of the Haiyuan earthquake and working to improve the ability of earthquake prediction and seismic hazard reduction," *Earthquake Research in China*, vol. 25, no. 3, pp. 260–272, 2011.

[49] H. F. Yang, D. Wang, R. M. Guo, et al., "Rapid report of the 8 January 2022 MS 6.9 Menyuan earthquake, Qinghai, China," *Earthquake Research Advances*, vol. 2, no. 1, p. 100113, 2022.

[50] J. W. Pan, H. B. Li, M. Chevalier, et al, "Coseismic surface rupture and Seismogenic structure of the 2022 Ms6.9 Menyuan earthquake, Qinghai province, China," *Acta Geologica Sinica (100th Anniversary)*, vol. 96, no. 1, pp. 215–231, 2022.

[51] P. Guo, Z. J. Han, Z. B. Mao, et al., "Paleoearthquakes and rupture behavior of the Lenglongling fault: Implications for seismic hazards of the Northeastern margin of the Tibetan plateau," *Journal of Geophysical Research*, vol. 124, no. 2, pp. 1520–1543, 2019.

[52] D. Y. Yuan, B. C. Liu, L. V. T. Y., W. G. He, and X. F. liu, "Palaeoearthquake features along the eastern segment of North Qilianshan active fault zone," *South China Journal of Seismology*, vol. 2, pp. 24–31, 1997.

[53] J. Liu-Zeng, Y. Klinger, X. W. Xu, et al., "Millennial recurrence of large earthquakes on the Haiyuan fault near Songshan, Gansu province, China," *Bulletin of the Seismological Society of America*, vol. 97, no. 1B, pp. 14–34, 2007.

[54] P. Z. Zhang, W. Min, Q. D. Deng, and F. Y. Mao, "Paleoearthquake rupture behavior and recurrence of great earthquakes along the Haiyuan fault, Northwestern China," *Science in China Series D*, vol. 48, no. 3, pp. 364–375, 2005.

[55] LIS (Lanzhou Institute of Seismology), *Quantitative Study and Seismic Risk Assessment of Seismogenic Active Structures in the Key Areas of the Middle to Eastern Qilian Mountains*, LIS (Lanzhou Institute of Seismology), Lanzhou, 2000.

[56] P. Guo, Z. J. Han, F. Gao, C. H. Zhu, and H. L. Gai, "A new Tectonic model for the 1927 M8.0 Gulang earthquake on the NE Tibetan plateau," *Tectonics*, vol. 39, no. 9, 2020.

[57] W. G. He, B. C. Liu, and D. Y. Yuan, "Preliminary study on Paleoearthquakes of Lenglongling fault," in *Research on Active Fault*, 8: Institute of Geology, China Earthquake Administration, Eds, pp. 64–73, Seismological Press, Beijing, 2001.

[58] P. Guo, Z. J. Han, W. L. Jiang, and Z. B. Mao, "Holocene left-lateral slip rate of the Lenglongling fault, northeastern margin of the Tibetan plateau," *Seismology and Geology*, vol. 39, no. 2, pp. 323–341, 2017.

[59] W. G. He, B. C. Liu, T. Y. Lu, D. Y. Yuan, and X. F. Liu, "The late Quaternary activity of the Maomaoshan fault Fone," in *Research on Active Fault*, 2: Institute of Geology, China Earthquake Administration, Eds, pp. 63–77, Seismological Press, Beijing, 1996.

[60] B. C. Liu, W. G. He, X. F. Liu, and D. Y. Yuan, "Study on the trench of Paleoearthquake in compressive ridge," in *Research on Active Fault*, 6: Institute of Geology, China Earthquake Administration, Eds, pp. 56–65, Seismological Press, Beijing, 1998.

[61] B. C. Liu, D. Y. Yuan, X. F. Liu, and W. G. He, "Late Quaternary Tectonic activity and Paleoearthquakes of Laohushan active fault," in *Research on Active Fault*, 3: Institute of Geology, China Earthquake Administration, Eds, pp. 58–66, Seismological Press, Beijing, 1994.

[62] W. J. Zheng, H. Y. Bi, X. L. Wang, et al., "Constraining Paleoearthquakes by combining faulted stratigraphy and Microgeomorphology: A case study on the Haiyuan fault, Northwestern China," *Seismological Research Letters*, vol. 92, no. 2A, pp. 895–908, 2021.

[63] W. Min, "Region Paleoearthquake research: an example in the Northeastern margin of Tibet and Western margin of Huabei," , (Doctor Thesis), Institute of Geology, China Earthquake Administrator, Beijing, 1998.

[64] IGCEA (Institute of Geology, China Earthquake Administrator), and NSBC (Ningxia Seismological Bureau of China), *"Haiyuan Active Fault Zone,"* Seismological Press, Beijing, 1990.

[65] W. Min, P. Z. Zhang, Q. D. Deng, and F. Y. Mao, "Detailed study of Holocene paleoearthquakes of the active Haiyuan fault," *Continental Dynamics*, vol. 6, no. 2, pp. 59–66, 2001.

[66] Y. K. Ran, R. T. Duan, Q. D. Deng, D. C. Jiao, and W. Min, "3d trench excavation and paleoseismology at Gaowanzi of the Haiyuan fault," *Seismology and Egology*, vol. 19, no. 2, pp. 97–107, 1997.

[67] Y. K. Ran, R. T. Duan, and Q. D. Deng, "Paleo- and strong earthquakes on major active segments along Haiyuan fault," in *Research on Active Fault*, 6: Institute of Geology, China Earthquake Administration, Eds, pp. 42–55, Seismological Press, Beijing, 1998.

[68] Y. B. Li, Y. K. Ran, H. Wang, and F. Y. Wu, "Paleoseismic records of large earthquakes on the cross-Basin fault in the Ganyanchi pull-apart Basin, Haiyuan fault, northeastern Tibetan plateau," *Natural Hazards*, vol. 71, no. 3, pp. 1695–1713, 2014.

[69] J. Liu-Zeng, Y. Shao, Y. Klinger, K. Xie, D. Yuan, and Z. Lei, "Variability in magnitude of paleoearthquakes revealed by trenching and historical records, along the Haiyuan fault, China," *Journal of Geophysical Research*, vol. 120, no. 12, pp. 8304–8333, 2015. https://onlinelibrary.wiley.com/toc/21699356/120/12.

[70] J. H. Yin, J. Chen, Y. T. Lu, and Y. G. Zheng, "The calendar date of paleo-earthquake event estimated by depth-age wiggle match," *Seismology and Geology*, vol. 23, no. 2, pp. 383–390, 2011.

[71] Z. Peizhen, P. Molnar, Z. Weigi, et al., "Bounds on the average recurrence interval of major earthquakes along the Haiyuan fault in North-central China," *Seismological Research Letters*, vol. 59, no. 3, pp. 81–89, 1988.

[72] W. Q. Zhang and D. C. Jiao, "A brief report on profiles of the Haiyuan Paleoearthquake," *Seismology and Geology*, vol. 6, no. 3, pp. 3–4, 1984.

[73] J. H. Yin, J. Chen, Y. G. Zheng, K. Q. Zhang, and Y. X. Liu, "The radiocarbon Ahes of charcoal and the implication derived from Ciergousite along the Haiyuan strike-slip fault," *Seismology and Geology*, vol. 27, no. 4, pp. 578–585, 2005.

[74] W. Min and S. P. Zhang, "A preliminary study on paleoearthquakes of Yueliangshan faults," *Northwestern Seismological Journal*, vol. 23, no. 1, pp. 36–40, 2001.

[75] H. F. Xiang, Y. Ikeda, W. X. Zhang, B. L. Zhang, S. M. Guo, and H. L. He, "Study on paleoearthquakes of the eastern Liupanshan piedmont fault zone," *Earthquake Research in China*, vol. 15, no. 1, pp. 74–91, 1999.

[76] P. J. Reimer, W. E. N. Austin, E. Bard, et al., "The Intcal20 northern hemisphere radiocarbon age calibration curve (0-55 Cal kBP)," *Radiocarbon*, vol. 62, no. 4, pp. 725–757, 2020.

[77] K. Aki, "Characterization of barriers on an earthquake fault," *Journal of Geophysical Research*, vol. 84, no. B11, p. 6140, 1979.

[78] K. Aki, "Asperities, barriers, characteristic earthquakes, and strong motion prediction," *Journal of Geophysical Research*, vol. 89, no. B7, pp. 5867–5872, 1984.

[79] S. G. Wesnousky, "Predicting the endpoints of earthquake Ruptures," *Nature*, vol. 444, no. 7117, pp. 358–360, 2006.

[80] S. G. Wesnousky, "Displacement and geometrical characteristics of earthquake surface Ruptures: Issues and implications for seismic-hazard analysis and the process of earthquake rupture," *Bulletin of the Seismological Society of America*, vol. 98, no. 4, pp. 1609–1632, 2008.

[81] Y. K. Ran, H. Wang, Y. B. Li, and L. C. Chen, "Key techniques and several cases analysis in paleoseismic studies in Mainland China(1): Trenching sites, layouts and paleoseismic indicators on active strike-slip faults," *Seismology and Geology*, vol. 34, no. 2, pp. 197–210, 2012.

[82] K. M. Scharer, R. J. Weldon, T. E. Fumal, and G. P. Biasi, "Paleoearthquakes on the Southern San Andreas fault, Wrightwood, California, 3000 to 1500 B.C.: A new method for evaluating paleoseismic evidence and earthquake horizons," *Bulletin of the Seismological Society of America*, vol. 97, no. 4, pp. 1054–1093, 2007.

[83] K. Scharer, R. Weldon, G. Biasi, A. Streig, and T. Fumal, "Ground-Rupturing earthquakes on the northern big bend of the San Andreas fault, California, 800 A.D. to present," *Journal of Geophysical Research*, vol. 122, no. 3, pp. 2193–2218, 2017. https://onlinelibrary.wiley.com/toc/21699356/122/3.

[84] Z. Yuan, J. Liu-Zeng, W. Wang, et al., "A 6000-year-long paleoseismologic record of earthquakes along the Xorkoli section of the Altyn Tagh fault, China," *Earth and Planetary Science Letters*, vol. 497, September, pp. 193–203, 2018.

[85] R. E. Wallace, "Profiles and ages of young fault Scarps, North-central Nevada," *Geological Society of America Bulletin*, vol. 88, no. 9, p. 1267, 1977.

[86] A. R. Nelson, "Holocene tidal-marsh stratigraphy in South-central Oregon: Evidence for localized sudden submergence in the Cascadia Subduction zone," *Quaternary Coasts of the United States: Marine and Lacustrine Systems, SEPM Special Publication*, vol. 48, pp. 287–301, 1992.

[87] C. R. Allen, L. Zhuoli, Q. Hong, W. Xueze, Z. Huawei, and H. Weishi, "Field study of a highly active fault zone: The Xianshuihe fault of Southwestern China," *Geological Society of America Bulletin*, vol. 103, no. 9, pp. 1178–1199, 1991.

[88] T. E. Fumal, D. P. Schwartz, S. K. Pezzopane, and R. J. Weldon 2nd, "A 100-year average recurrence interval for the San Andreas fault at Wrightwood, California," *Science (New York, N.Y.)*, vol. 259, no. 5092, pp. 199–203, 1993.

[89] M. G. Bonilla and J. J. Lienkaemper, *"Factors Affecting the Recognition of Faults Exposed in Exploratory Trenches,"* United States Government Printing Office, Washington, 1991.

[90] J. P. McCalpin, "Late Quaternary activity of the Pajarito fault, Rio Grande rift of northern New Mexico, USA," *Tectonophysics*, vol. 408, nos. 1–4, pp. 213–236, 2005.

[91] N. Khajavi, R. M. Langridge, M. C. Quigley, C. Smart, A. Rezanejad, and F. Martín-González, "Late Holocene rupture behavior and earthquake chronology on the hope fault, New Zealand," *Geological Society of America Bulletin*, vol. 128, nos. 11–12, pp. 1736–1761, 2016.

[92] K. M. Scharer and D. Yule, "A maximum rupture model for the Southern San Andreas and San Jacinto faults, California, derived from paleoseismic earthquake ages: Observations and limitations," *Geophysical Research Letters*, vol. 47, no. 15, 2020.

[93] C. B. DuRoss, R. D. Gold, H. J. Gray, and S. R. Nicovich, "Portable optically stimulated luminescence age map of a paleoseismic exposure," *Geology*, vol. 50, no. 4, pp. 470–475, 2022.

[94] Q. D. Deng, W. Q. Zhang, P. Z. Zhang, et al., "Haiyuan strike-slip fault zone and its compressional structures at the end," *Seismology and Geology*, vol. 11, no. 1, pp. 1–14, 1989.

[95] S. Lei, Y. Li, E. Cowgill, et al., "Magnetostratigraphy of the Ganyanchi (salt Lake) Basin along the Haiyuan fault, northeastern Tibet," *Geosphere*, vol. 14, no. 5, pp. 2188–2205, 2018.

[96] R. A. Harris and S. M. Day, "Dynamics of fault interaction: Parallel strike-slip faults," *Journal of Geophysical Research*, vol. 98, no. B3, pp. 4461–4472, 1993.

[97] R. A. Harris and S. M. Day, "Dynamic 3d simulations of earthquakes on en echelon faults," *Geophysical Research Letters*, vol. 26, no. 14, pp. 2089–2092, 1999.

[98] P. Z. Zhang, F. Y. Mao, and D. B. Slemmons, "Rupture terminations and size of segment boundaries from historical earthquake Ruptures in the basin and range province," *Tectonophysics*, vol. 308, nos. 1–2, pp. 37–52, 1999.

[99] E. Cowgill, A. Yin, J. R. Arrowsmith, W. X. Feng, and Z. Shuanhong, "The Akato Tagh bend along the Altyn Tagh fault, northwest Tibet 1: Smoothing by vertical-axis rotation and the effect of topographic stresses on bend-flanking faults," *Geological Society of America Bulletin*, vol. 116, nos. 11–12, pp. 1423–1442, 2004.

[100] B. C. Duan and D. D. Oglesby, "Multicycle dynamics of nonplanar strike-slip faults," *Journal of Geophysical Research*, vol. 110, no. B3, p. article B03304 , 2005.

[101] J. D. Howarth, N. C. Barth, S. J. Fitzsimons, et al., "Spatiotemporal clustering of great earthquakes on a transform fault controlled by geometry," *Nature Geoscience*, vol. 14, no. 5, pp. 314–320, 2021.

[102] S. M. Liang, W. J. Zheng, D. L. Zhang, et al., "Paleoearthquakes constrained by stratigraphic sequences of different drainages since late pleistocene: A case study along the Gulang fault, NE Tibetan plateau," *Frontiers in Earth Science*, vol. 9, 2021

[103] Y. Klinger, M. Etchebes, P. Tapponnier, and C. Narteau, "Static characteristic slip for five great earthquakes along the Fuyun fault in China," *Nature Geoscience*, vol. 4, no. 6, pp. 389–392, 2011.

[104] Z. K. Ren, Z. Q. Zhang, T. Chen, et al., "Lustering of offsets on the Haiyuan fault and their relationship to Paleoearthquakes," *Geological Society of America Bulletin*, vol. 128, nos. 1–2, 2016.

[105] Zielke, O., Klinger, Y., and Arrowsmith, J. R., "Fault slip and earthquake recurrence along strike-slip faults — Contributions of high-resolution geomorphic data", Tectonophysics, vol. 638, pp. 43–62, 2015.

[106] H. Y. Bi, W. J. Zheng, P. Z. Zhang, et al., "Recovering surface slip distribution along the sertengshan piedmont fault (northern China) from airborne Lidar data," *Tectonics*, vol. 41, no. 8, 2022.

[107] J. X. Zhou, T. X. Yang, J. Y. Yao, J. Liu., and B. C. Liu, "The fracture belt of Gulang earthquake on May, 23 in 1927 in Gansu province," *Northwestern Seismological Journal*, vol. 8, no. 3, pp. 114–115, 1986.

[108] W. J. Zheng, D. Y. Yuan, and W. G. He, "Characteristics of paleoseismic activity along the Tianqiaogou–Huangyangchuan fault on the Eastern section of the Qilian mountains," *Earthquake Research in China*, vol. 19, no. 2, pp. 139–151, 2005.

[109] D. L. Wells and K. J. Coppersmith, "New empirical relationships among magnitude, rupture length, rupture width, rupture area, and surface displacement," *Bulletin of the Seismological Society of America*, vol. 84, no. 4, pp. 974–1002, 1994.

[110] Y. Gaudemer, P. Tapponnier, B. Meyer, et al., "Partitioning of Crustal slip between linked, active faults in the Eastern Qilian shan, and evidence for a major seismic gap, the 'Tianzhu gap', on the Western Haiyuan fault, Gansu (China)," *Geophysical Journal International*, vol. 120, no. 3, pp. 599–645, 1995.

[111] C. Lasserre, P.-H. Morel, Y. Gaudemer, et al., "Postglacial left slip rate and past occurrence of M ≥8 earthquakes on the Western Haiyuan fault, Gansu, China," *Journal of Geophysical Research*, vol. 104, no. B8, pp. 17633–17651, 1999.

[112] C. Lasserre, Y. Gaudemer, P. Tapponnier, et al., "Fast late Pleistocene slip rate on the Leng long LING segment of the Haiyuan fault, Qinghai, China," *Journal of Geophysical Research*, vol. 107, no. B11, 2002.

[113] R. Jolivet, C. Lasserre, M.-P. Doin, et al., "Shallow creep on the Haiyuan fault (Gansu, China) revealed by SAR Interferometry," *Journal of Geophysical Research*, vol. 117, no. B6, 2012.

[114] Y. C. Li, X. J. Shan, C. Y. Qu, and Z. J. Wang, "Fault locking and slip rate deficit of the Haiyuan-Liupanshan fault zone in the Northeastern margin of the Tibetan plateau," *Journal of Geodynamics*, vol. 102, December, pp. 47–57, 2016.

[115] R. E. Wallace, "Earthquake recurrence intervals on the San Andreas fault," *Geological Society of America Bulletin*, vol. 81, no. 10, p. 2875, 1970.

[116] M. N. Toksöz, A. F. Shakal, and A. J. Michael, "Space-time migration of earthquakes along the North Anatolian fault zone and seismic gaps," *Pure and Applied Geophysics PAGEOPH*, vol. 117, no. 6, pp. 1258–1270, 1979.

[117] N. Pondard, R. Armijo, G. C. P. King, B. Meyer, and F. Flerit, "Fault interactions in the sea of Marmara pull-apart (North Anatolian fault): earthquake clustering and Propagating earthquake sequences," *Geophysical Journal International*, vol. 171, no. 3, pp. 1185–1197, 2007.

[118] C. H. Scholz, "Large earthquake triggering, clustering, and the synchronization of faults," *Bulletin of the Seismological Society of America*, vol. 100, no. 3, pp. 901–909, 2010.

[119] D. P. Schwartz, J. J. Lienkaemper, S. Hecker, et al., "The earthquake cycle in the San Francisco Bay region: A.D. 1600-2012," *Bulletin of the Seismological Society of America*, vol. 104, no. 3, pp. 1299–1328, 2014.

[120] B. Philibosian and A. J. Meltzner, "Segmentation and Supercycles: A catalog of earthquake rupture patterns from

the Sumatran Sunda Megathrust and other well-studied faults worldwide," *Quaternary Science Reviews*, vol. 241, August, p. 106390, 2020.

[121] Q. Zhang, P. Zhang, C. Wang, Y. Wang, and M. A. Ellis, "Earthquake triggering and delaying caused by fault interaction on Xianshuihe fault belt, Southwestern China," *Acta Seismologica Sinica*, vol. 16, no. 2, pp. 156–165, 2003.

[122] N. Kato, X. L. Lei, and X. Z. Wen, "A synthetic Seismicity model for the Xianshuihe fault, Southwestern China: simulation using a Rate- and state-dependent friction law," *Geophysical Journal International*, vol. 169, no. 1, pp. 286–300, 2007. http://blackwell-synergy.com/doi/abs/10.1111/gji.2007.169.issue-1.

[123] X. L. Lei, S. L. Ma, J. R. Su, and X. L. Wang, "Inelastic triggering of the 2013 Mw 6.6 Lushan earthquake by the 2008 Mw 7.9 Wenchuan earthquake," *Seismology and Geology*, vol. 35, no. 2, pp. 411–422, 2013.

[124] Q. D. Deng, P. Z. Zhang, Y. K. Ran, X. P. Yang, W. Min, and Q. Z. Chu, "Basic characteristics of active tectonics of China," *Science in China (Series D)*, vol. 46, no. 4, pp. 356–372, 2003.

[125] W. Yao, J. Liu-Zeng, M. E. Oskin, et al., "Reevaluation of the late Pleistocene slip rate of the Haiyuan fault near Songshan, Gansu province, China," *Journal of Geophysical Research*, vol. 124, no. 5, pp. 5217–5240, 2019.

[126] B. C. Liu, T. Y. Lv, D. Y. Yuan, et al, *Laohushan, Maomaoshan and Jinqianghe Fault in the Eastern Part of Qilian Active Fault*, Seismological Press, Beijing, 2013.

[127] T. Chen, P. Z. Zhang, J. Liu, C. Y. Li, Z. K. Ren, and K. W. Hudnut, "Quantitative study of tectonic geomorphology along Haiyuan fault based on airborne LiDAR," *Chinese Science Bulletin*, vol. 59, no. 20, pp. 2396–2409, 2014.